General Disclaimer

One or more of the Following Statements may affect this Document

- This document has been reproduced from the best copy furnished by the organizational source. It is being released in the interest of making available as much information as possible.

- This document may contain data, which exceeds the sheet parameters. It was furnished in this condition by the organizational source and is the best copy available.

- This document may contain tone-on-tone or color graphs, charts and/or pictures, which have been reproduced in black and white.

- This document is paginated as submitted by the original source.

- Portions of this document are not fully legible due to the historical nature of some of the material. However, it is the best reproduction available from the original submission.

NASA CR-144969

A Theoretical Investigation of Over-Wing-Blowing Aerodynamics

by

C. Edward Lan

Technical Report KU-FRL-700

March 1976

The Flight Research Laboratory

Department of Aerospace Engineering

The University of Kansas

Lawrence, Kansas 66045

Prepared under NASA Grant NSG 1139

for

National Aeronautics and Space Administration

TABLE OF CONTENTS

Summary

A theoretical method is established for determining the aerodynamic characteristics of over-wing-blowing configurations. The method accounts for both jet entrainment and jet interaction effects because of the differences in freestream and jet dynamic pressures and Mach numbers. The predicted lift increments agree well with available data. It is shown that the lift is underpredicted with entrainment effect alone when the jet is close to the wing surface.

1. Introduction

The over-wing engine installation has recently been investigated as an alternative of installing high by-pass ratio turbofan engines. With the conventional under-wing installation, these big engines may have ground clearance problem and adverse aerodynamic effects on the wing. In addition to solving the ground clearance problem, the over-wing installation has the advantages of reducing jet noise because of wing shielding effect and improving the aerodynamic performance. In some experimental investigations, Bagley and his associates tested a model with rectangular jet nozzle at high subsonic freestream Mach numbers [Refs. 1 and 2]. Similarly, extensive experimental study of various configurations has been made at VFW-Fokker in connection with the VFW-614 project [Ref. 3]. In the test configurations mentioned above, the nacelles were installed directly above the wing. Therefore, the nacelle-pylon solid-body interference on the wing flow will be significant. On the other hand, Seidel [Ref. 4] and Putnam [Ref. 5] measured wing aerodynamic characteristics with the jet exit ahead of the wing leading edge. Seidel also allowed the blowing jet to be inclined relative to the freestream. From these limited experiments, the favorable aerodynamic effects of the over-wing blowing jets have been confirmed.

In general, when a turbulent jet is blowing above the wing, the wing upwash will be increased due to jet entrainment. The jet entrainment effect on the wing can be simulated by using sink distribution along the jet axis. For this purpose, Squire and Trouncer [Ref. 6] derived a theoretical sink strength distribution for incompressible, non-heated jets. This theory has been used to estimate the jet effects on the horizontal tail [Ref. 7].

Ribner extended Squire and Trouncer's analysis to heated but incompressible jets [Ref. 8]. In these early investigations, the primary objective has been the study of jet entrainment effects on the tail. On the other hand, Putnam [Ref. 9] has recently applied Squire and Trouncer's theory to the investigation of the wing aerodynamic characteristics due to over-wing blowing jets at moderate to high subsonic Mach numbers. Because the theory is applicable only to incompressible flow, Putnam used equivalent incompressible jet parameters in his applications. Line sink distribution was used in conjunction with the vortex-lattice method. Another approach used at VFW-Fokker was to use sink panels over the jet surface [Ref. 3]. Both the sink strength and the jet boundary for the velocity ratio V_o/V_j of 1/7 were based on the static jet properties, so that the entrainment used in the computation is expected to be higher than the actual magnitude. In both investigations, it has been indicated that when the jet is close to the wing surface, the methods would be inadequate. In fact, the predicted lift due to entrainment alone would be too low as compared with the experiments [Ref. 9]. Therefore, additional lift mechanism must be examined.

In the present investigation, the lift induced by the over-wing blowing jets will be shown to be attributable to the jet entrainment and the inviscid jet-wing interaction due to the higher dynamic pressure in the jet. The latter effect is particularly important when the jet is close to the wing surface. To extend the capability of existing methods for computing jet entrainment to compressible heated jets, Kleinstein's theory for static compressible jets [Ref. 10] is extended to the case of external stream, with the simplicity of his theory being retained. The wing-jet interaction theory with Mach number nonuniformity reported earlier [Ref. 11] will then be used to treat the interaction between the wing and a rectangular or a round jet.

2. List of Symbols

AR	wing aspect ratio
$\bar{b}_{1/2}$	nondimensional turbulent jet half width defined in Eq. A.21
c	local chord length, m (ft)
$\bar{c}$	reference chord length, m (ft)
C	leading-edge singularity parameter (see Eq. (27))
c_{d_i}	sectional induced drag coefficient
c_f	flap-chord length, m (ft)
c_ℓ	sectional lift coefficient
ΔC_L	difference in lift coefficients with jet on and off
c_m	sectional pitching-moment coefficient about y-axis
C_p	pressure coefficient, or specific heat at constant pressure
c_t	sectional leading-edge thrust coefficient
d_o	initial jet diameter, m (ft)
$\vec{e}$	unit vector tangent to jet path and is taken to be $\vec{i}$ in the shallow jet approximation
E(x)	entrainment function defined in Eq. A.65
F_1	a function defined by Eq. A.11
F_2	a function defined by Eq. A.12
F_3	a function defined by Eq. A.38
H	stagnation enthalpy
$\vec{i},\vec{j},\vec{k}$	unit vector along x-, y- and z-axes, respectively
k_1	a constant in Ferri's turbulent eddy viscosity model (see Eq. A.20)

m	mass flow rate, kg/sec (slugs/sec)
m'	slope
M	Mach number, or momentum
N	number of chordwise integration points
$[N]$	normal velocity influence-coefficient matrix
$\vec{n}$	unit vector normal to the jet surface
n,s	jet axis system with n normal to the surface and s tangential to it
p_∞	free stream static pressure, N/m^2 (lb/ft^2)
$p_{t,j}$	jet stagnation pressure, N/m^2 (lb/ft^2)
$P_o(x)$	a function defined by Eq. A.16
$P_1(x)$	a function defined by Eq. A.10
$P_2(x)$	a function defined by Eq. A.13
q	entrained volume flow rate, m^3/sec (ft^3/sec)
r	radial coordinate, m (ft)
$\tilde{r}_j$	equivalent jet radius, m (ft)
r_o	initial jet radius, m(ft)
$\bar{R}$	average gas constant for the air-jet mixture
R_j	gas constant for the jet
S	wing area, m^2 (ft^2)
$[S]$	tangential velocity influence-coefficient matrix
t	airfoil thickness, m (ft)
T	temperature, °K (°R)
$\bar{T}$	$= p_o/\rho_j$
$T_{t,j}$	jet stagnation temperature, °K (°R)

$T_{t,\infty}$ free stream stagnation temperature, °K (°R)

u velocity in x-direction, m/sec (ft/sec)

$\bar{u}$ $= u/u_j$

$\tilde{u}_j$ equivalent jet velocity, m/sec (ft/sec)

V velocity, m/sec (ft/sec)

$\vec{V}$ unperturbed velocity vector, m/sec (ft/sec)

v perturbed velocity vector, m/sec (ft/sec)

$\vec{v}_{je}$ jet-entrained-flow velocity vector, m/sec (ft/sec)

$\bar{x}$ $= x/r_o$

$\bar{x}_c$ nondimensional turbulent jet potential core length based on r_o

x_j, z_j jet exit x- and z-coordinates

x,y,z wing-fixed rectangular coordinate with positive x-axis along axis of symmetry pointing downstream, positive y-axis pointing to right and positive z-axis pointing upward, m (ft)

z_c coordinate of camber surface, $z_c = z_c(x,y)$, m (ft)

α angle of attack, deg

β $= (1-M^2)^{\frac{1}{2}}$

γ nondimensional vortex density, or ratio of specific heats

δ_e airfoil trailing-edge half angle, deg

δ_j jet deflection angle, deg

ξ_1 $= r/r_j$

θ $= T_j/T_e$

$\bar{\theta}(x)$ angle of camber slope

Λ sweep angle, deg

μ $= V_o/V_j$, or u_o/u_j

μ' $= \vec{V}_o.\vec{e}/\vec{V}_j.\vec{e}$

ρ density, kg/m^3 (slugs/ft^3)

$\tilde{\rho}_j$ equivalent jet density, kg/m^3 (slugs/ft^3)

$\overline{\rho\varepsilon}$ nondimensional turbulent transfer coefficient

ϕ dimensional perturbation velocity potential, m^2/sec (ft^2/sec)

$\overline{\phi}$ nondimensional perturbation velocity potential

ψ nondimensional additional perturbation velocity potential, or stream function

Subscripts:

a additional

c jet centerline

e external or outer flow

j jet flow

jj jet vortices for jet flow

ℓ leading edge

o outer or external flow

oj jet vortices for outer flow

t trailing edge

w wing

wa additional wing vortices

wj perturbation due to wing in jet flow

wo perturbation due to wing in outer flow

∞ free stream

3. Mathematical Formulation

3.1 Inviscid Interaction

In general, a jet will expand after leaving the nozzle and its axial velocity will decay downstream. The velocity distribution over any jet section is nonuniform, with maximum value at the center. For simplicity, an equivalent jet section with uniform velocity distribution, to be defined later, will be used in the present formulation. Since the jet flow has higher dynamic pressure than the freestream, any disturbances created outside the jet will be reflected and diffracted at the jet surface [Ref. 12]. The disturbances in the present applications are mainly due to the presence of the wing in the freestream and the jet-entrained flow. This inviscid wing-jet interaction is the subject of formulation in the present section.

The perturbations of the flow field mentioned above are determined by satisfying the boundary conditions. On the jet surface, it is required that the slopes of the streamlines on both sides of the surface are the same. When linearized, this condition can be expressed as [Ref. 11]

$$\vec{V}_o \cdot \vec{n}\,(1-\mu') + \frac{\partial \phi_o}{\partial n} \approx \mu' \frac{\partial \phi_j}{\partial n} \qquad (1)$$

One additional jet surface boundary condition is the static pressure continuity, which in linearized version can be written as

$$S_j (\vec{V}_j \cdot \vec{e}) \frac{\partial \phi_j}{\partial s} \approx S_o (\vec{V}_o \cdot \vec{e}) \frac{\partial \phi_o}{\partial s} \qquad (2)$$

In the above, $\vec{e}$ is a unit vector tangent to the jet path and is taken to be $\vec{i}$ in the shallow jet approximation, and $\vec{n}$ is the unit vector normal to the surface. $\vec{V}_j$ is the unperturbed jet velocity and $\vec{V}_o$ is the external velocity vector before the wing is introduced into the flow field.

With the wing being assumed to be entirely in the outer-flow region, the wing tangency condition has the conventional form:

$$\frac{\partial \phi_o}{\partial z} = (\vec{V}_o \cdot \vec{i}) \frac{\partial z_c}{\partial x} - \vec{V}_o \cdot \vec{k} \tag{3}$$

For numerical convenience, Eqs. (1)-(3) will first be rewritten in a nondimensional form. For this purpose, define the nondimensional perturbation potentials $\bar{\phi}_o$ and $\bar{\phi}_j$ such that

$$\phi_o = (\vec{V}_o \cdot \vec{e})\, \bar{\phi}_o \tag{4}$$

$$\phi_j = (\vec{V}_j \cdot \vec{e})\, \bar{\phi}_j \tag{5}$$

Introducing Eqs. (4)-(5) into Eqs. (1)-(3), it is obtained with some simplification that

$$\frac{\partial \bar{\phi}_o}{\partial n} - \frac{\partial \bar{\phi}_j}{\partial n} = -\frac{\vec{V}_o \cdot \vec{n}\,(1-\mu')}{\vec{V}_o \cdot \vec{e}} \tag{6}$$

$$\frac{\partial \bar{\phi}_j}{\partial s} - \bar{T}(\mu')^2 \frac{\partial \bar{\phi}_o}{\partial s} = 0 \tag{7}$$

$$\frac{\partial \bar{\phi}_o}{\partial z} = \frac{\vec{V}_o \cdot \vec{i}}{\vec{V}_o \cdot \vec{e}} \frac{\partial z_c}{\partial x} - \frac{\vec{V}_o \cdot \vec{k}}{\vec{V}_o \cdot \vec{e}} \tag{8}$$

where

$$\bar{T} = \rho_o / \rho_j \tag{9}$$

Let $\vec{V}_{je}$ be the jet-entrained flow and $\vec{V}_\infty$ the uniform freestream vector. Then

$$\vec{V}_o = \vec{V}_\infty + \vec{V}_{je} \tag{10}$$

It is assumed that the jet-entrained flow does not affect the jet stream surface condition (Eq. 6) in the interaction formulation. It influences only the wing tangency condition through Eq. (8). Since the problem is linear, it is convenient to decompose it into the wing-alone case and the additional jet-induced perturbation. Therefore, let

$$\bar{\phi}_o = \bar{\phi}_{wo}(M_o) + \psi_o(M_o) \tag{11}$$

$$\bar{\phi}_j = \bar{\phi}_{wj}(M_j) + \psi_j(M_j) \tag{12}$$

where $\bar{\Phi}_{wo}(M_o)$ and $\bar{\Phi}_{wj}(M_j)$ are the wing-alone perturbation potentials at respective Mach numbers. Using Eqs. (11)-(12), Eqs. (6)-(8) become

$$\frac{\partial \psi_o}{\partial n} - \frac{\partial \psi_j}{\partial n} = -\frac{\vec{V}_\infty \cdot \vec{n}\,(1-\mu')}{\vec{V}_\infty \cdot \vec{e}} + \frac{\partial \bar{\Phi}_{wj}(M_j)}{\partial n} - \frac{\partial \bar{\Phi}_{wo}(M_o)}{\partial n} \tag{13}$$

$$\frac{\partial \psi_j}{\partial s} - \bar{T}(\mu')^2 \frac{\partial \psi_o}{\partial s} = -\frac{\partial \bar{\Phi}_{wj}}{\partial s} + \bar{T}(\mu')^2 \frac{\partial \bar{\Phi}_{wo}}{\partial s} \tag{14}$$

$$\frac{\partial \psi_o}{\partial z} = 0 \tag{15}$$

where $\bar{\Phi}_{wo}$ and $\bar{\Phi}_{wj}$ satisfy the conventional tangency condition with jet entrainment:

$$\frac{\partial \bar{\Phi}_{wo}(M_o)}{\partial z} = \frac{\partial z_c}{\partial x} - \tan\alpha - \frac{\vec{v}_{je} \cdot \vec{k}}{V_\infty \cos\alpha} \tag{16}$$

$$\frac{\partial \bar{\Phi}_{wj}(M_j)}{\partial z} = \frac{\partial z_c}{\partial x} - \tan\alpha - \frac{\vec{v}_{je} \cdot \vec{k}}{V_\infty \cos\alpha} \tag{17}$$

Because of Mach number nonuniformity, two vortex sheets are introduced on the jet surface, one with strength γ_{oj} to account for the outer flow perturbation and the other with strength γ_{jj} to account for the jet flow perturbation. Let γ_{wa} be the additional wing vortex strength. Then Eqs. (13)-(15) can be reduced to [Ref. 11]

$$[N_{JW}]_{(o)}\{\gamma_{wa}\} + [N_{JJ}]_{(o)}\{\gamma_{oj}\} - [N_{JJ}]_{(j)}\{\gamma_{jj}\} = \left\{-\frac{\vec{V}_\infty \cdot \vec{n}\,(1-\mu')}{\vec{V}_\infty \cdot \vec{e}} + \frac{\partial \bar{\Phi}_{wj}}{\partial n}(M_j) - \frac{\partial \bar{\Phi}_{wo}}{\partial n}(M_o)\right\} \tag{18}$$

$$-\bar{T}(\mu')^2[S_{JW}]_{(o)}\{\gamma_{wa}\} - \bar{T}(\mu')^2[S_{JJ}]_{(o)}\{\gamma_{oj}\} + [S_{JJ}]_{(j)}\{\gamma_{jj}\} = \left\{-\frac{\partial \bar{\Phi}_{wj}}{\partial s} + \bar{T}(\mu')^2 \frac{\partial \bar{\Phi}_{wo}}{\partial s}\right\} \tag{19}$$

$$[N_{WW}]\{\gamma_{wa}\} + [N_{WJ}]_{(o)}\{\gamma_{oj}\} = 0 \tag{20}$$

where [N] and [S] are the influence coefficient matrices for induced normal and tangential velocity components, with the first subscript denoting the control point locations and the second for the influencing vortex locations. When the jet is close enough to the wing, it may

attach to the wing upper surface due to the Coanda effect. As a result, the jet may deflect at the wing trailing edge. This jet flap effect can be included in accordance with method described in Ref. 11. Both [N] and [S] matrices are formulated with the Quasi Vortex-Lattice Method (Quasi VLM) (Ref. 13). Since the Quasi VLM is one type of the discrete-element methods, care must be taken in evaluating [S] matrices for better accuracy (Ref. 11).

Once Eqs. (18)-(20) have been solved, the total wing vortex strength is given by

$$\gamma_w = \gamma_{wo} + \gamma_{wa} \tag{21}$$

The sectional wing aerodynamic characteristics can be computed by properly resolving the pressure force acting on the camber surface into appropriate directions. It follows that

$$c_\ell = \frac{1}{\frac{1}{2}\rho_\infty V_\infty^2 c}\int_{x_\ell}^{x_t} \rho_\infty V_\infty (\vec{V}_\infty \cdot \vec{e})\,\gamma_w(x)\cos(\alpha - \bar{\theta}(x))\,dx + c_t \sin(\alpha - \bar{\theta}_\ell)$$

$$= \frac{2\cos\alpha}{c}\int_{x_\ell}^{x_t}\gamma_w(x)\cos(\alpha-\bar{\theta}(x))\,dx + c_t\sin(\alpha-\bar{\theta}_\ell) \tag{22}$$

$$c_{d_i} = \frac{2\cos\alpha}{c}\int_{x_\ell}^{x_t}\gamma_w(x)\sin(\alpha-\bar{\theta}(x))\,dx - c_t\cos(\alpha-\bar{\theta}_\ell) \tag{23}$$

$$c_m = \frac{2\cos\alpha}{\bar{c}\,c}\int_{x_\ell}^{x_t}\gamma_w(x)\,x\cos(\alpha-\bar{\theta}(x))\,dx \tag{24}$$

where

$$\bar{\theta}(x) = \tan^{-1}\left(\frac{dz_c}{dx}\right) \tag{25}$$

The sectional leading-edge thrust coefficient c_t is computed as (Ref. 13)

$$c_t = \frac{\pi}{2\cos\Lambda_\ell}\left(1 - M_\infty^2\cos^2\Lambda_\ell\right)^{1/2} C^2 \tag{26}$$

where the leading-edge singularity parameter C is defined as

$$C = \lim_{\theta\to 0}\frac{1}{2}\gamma(\theta)\sin\theta \tag{27}$$

According to the Quasi VLM, C can be determined by summing the total induced normal velocity at the leading edge and subtracting the right-hand side of Eq. (17) or (20), depending on whether the effects of wing alone or the jet interaction is being considered. If the induced normal velocity at the ith leading edge control point is denoted by a subscript i, then the singularity parameter C_1 in the wing alone case with flap deflection can be computed from the expression:

$$N_1 C_1 \left[(x_f - x_\ell)/c\right]^{-1/2} (\tan^2\Lambda_\ell + \beta^2)^{1/2} = [N_{ww}]_i \{\gamma_{wo}\} - \left\{\frac{\partial z_c}{\partial x} - \tan\alpha\right\}_i \qquad (28)$$

Similarly, the singularity parameter, C_2 due to the jet-induced perturbation can be computed from Eq. (29):

$$N_1 C_2 \left[(x_f - x_\ell)/c\right]^{-1/2} (\tan^2\Lambda_\ell + \beta^2)^{1/2} = [N_{ww}]_i \{\gamma_{wa}\} + [N_{wJ}]_{(\omega)i} \{\gamma_{oj}\} \qquad (29)$$

In the above, N_1 is the chordwise number of vortex elements on the airfoil section. The integrals in Eqs. (22)-(24) are computed with the midpoint trapezoidal rule after the θ-transformation. The overall aerodynamic characteristics of the wing are then determined by spanwise integration of the sectional characteristics (Ref. 11).

3.2 The Jet Entrainment Model

The jet entrainment affects the wing aerodynamic characteristics by creating additional upwash on the wing. This additional upwash is represented by the last term in Eq. (16) or (17). The ability of predicting the jet-entrained flow in subsonic compressible flow is important in the present investigation. Although it is possible to solve the jet problem by numerically integrating the governing equations (Ref. 14), such an approach would greatly increase the total computing time. With the idea of having a method being simple, general

and accurate in mind, it appears that Kleinstein's theory (Ref. 10) is the best choice. However, Kleinstein presented his theory for free jets only. In Appendix A, a method is described to extend Kleinstein's theory to compressible jets in an external stream, with the primary end results being the prediction of jet entrainment.

As shown in Appendix A, the entrained mass flow rate is computed as $\partial m/\partial x$ (See Eq. A.42). Let the entrained volume flow rate be denoted by q:

$$q_b = \frac{1}{\rho_j}\frac{\partial m}{\partial x} \tag{30}$$

The effects of the jet entrainment on the nearby lifting surfaces can be simulated by a line sink distribution on the jet axis with strength equal to the entrained volume flow rate. The induced velocity components due to this sink distribution can be computed as (Ref. 15)

$$\frac{\partial \phi}{\partial \bar{r}} = -\frac{\beta^2 \bar{r}}{4\pi}\int_0^{\infty}\frac{q_b(\bar{\xi})\,d\bar{\xi}}{[(\bar{x}-\bar{\xi})^2+\beta^2\bar{r}^2]^{3/2}} \tag{31}$$

$$\frac{\partial \phi}{\partial \bar{x}} = -\frac{1}{4\pi}\int_0^{\infty}\frac{q_b(\bar{\xi})(\bar{x}-\bar{\xi})\,d\bar{\xi}}{[(\bar{x}-\bar{\xi})^2+\beta^2\bar{r}^2]^{3/2}} \tag{32}$$

Instead of using q directly, it is convenient to use the nondimensional entrainment function $E(\bar{x})$ defined as (Ref. 16)

$$\frac{d_o}{m_j}\left(\frac{\rho_j}{\rho_e}\right)^{1/2}\frac{\partial m}{\partial x} = E(\bar{x}) \tag{33}$$

Hence

$$q_b = \frac{1}{\rho_j}E(\bar{x})\frac{m_j}{d_o}(\bar{\rho}_e)^{1/2} = \frac{\pi}{2}u_j r_o(\bar{\rho}_e)^{1/2}E(\bar{x}) \tag{34}$$

In applications, Eqs. (31) and (32) can be integrated by dividing the jet axis into segments within each of which $E(\bar{\xi})$ is assumed to vary linearly. Let

$$E(\bar{\xi}) = a_i + b_i\bar{\xi} \tag{35}$$

in the ith interval. Then

$$\frac{\partial \phi}{\partial \bar{r}} = -\frac{1}{4\pi}\beta^2 \bar{r}\,\frac{\pi}{2}\,u_j r_0 \left(\bar{S}_e\right)^{1/2} \sum_i \int_{\bar{x}_i}^{\bar{x}_{i+1}} \frac{(a_i + b_i \bar{\xi})\, d\bar{\xi}}{\left[(\bar{x}-\bar{\xi})^2 + \beta^2 \bar{r}^2\right]^{3/2}}$$

or,

$$\frac{1}{u_j r_0}\frac{\partial \phi}{\partial \bar{r}} = -\frac{\left(\bar{S}_e\right)^{1/2}}{8}\beta^2 \bar{r} \sum_i \int_{\bar{x}_i}^{\bar{x}_{i+1}} \frac{(a_i + b_i \bar{\xi})\, d\bar{\xi}}{\left[(\bar{x}-\bar{\xi})^2 + \beta^2 \bar{r}^2\right]^{3/2}} \tag{36}$$

Similarly,

$$\frac{1}{u_j r_0}\frac{\partial \phi}{\partial \bar{x}} = -\frac{\left(\bar{S}_e\right)^{1/2}}{8} \sum_i \int_{\bar{x}_i}^{\bar{x}_{i+1}} \frac{(a_i + b_i \bar{\xi})(\bar{x}-\bar{\xi})\, d\bar{\xi}}{\left[(\bar{x}-\bar{\xi})^2 + \beta^2 \bar{r}^2\right]^{3/2}} \tag{37}$$

The integrals in Eqs. (36) and (37) can be exactly integrated to give

$$\int_{\bar{x}_i}^{\bar{x}_{i+1}} \frac{(a_i + b_i \bar{\xi})\, d\bar{\xi}}{\left[(\bar{x}-\bar{\xi})^2 + \beta^2 \bar{r}^2\right]^{3/2}} = -\frac{a_i + b_i \bar{x}}{\beta^2 \bar{r}^2} G_{1i} - b_i G_{2i} \tag{38}$$

$$\int_{\bar{x}_i}^{\bar{x}_{i+1}} \frac{(a_i + b_i \bar{\xi})(\bar{x}-\bar{\xi})}{\left[(\bar{x}-\bar{\xi})^2 + \beta^2 \bar{r}^2\right]^{3/2}} d\bar{\xi} = (a_i + b_i \bar{x}) G_{2i} - b_i G_{1i} + b_i \ln \frac{\bar{x} - \bar{x}_{i+1} + \sqrt{(\bar{x}-\bar{x}_{i+1})^2 + \beta^2 \bar{r}^2}}{\bar{x} - \bar{x}_i + \sqrt{(\bar{x}-\bar{x}_i)^2 + \beta^2 \bar{r}^2}} \tag{39}$$

where

$$G_{1i} = \frac{\bar{x} - \bar{x}_{i+1}}{\sqrt{(\bar{x}-\bar{x}_{i+1})^2 + \beta^2 \bar{r}^2}} - \frac{\bar{x} - \bar{x}_i}{\sqrt{(\bar{x}-\bar{x}_i)^2 + \beta^2 \bar{r}^2}} \tag{40}$$

$$G_{2i} = \frac{1}{\sqrt{(\bar{x}-\bar{x}_{i+1})^2 + \beta^2 \bar{r}^2}} - \frac{1}{\sqrt{(\bar{x}-\bar{x}_i)^2 + \beta^2 \bar{r}^2}} \tag{41}$$

Note that only $\frac{\partial \phi}{\partial \bar{r}}$ -component will contribute to an upwash on the wing. To find $\vec{v}_{je} \cdot \vec{n}$ in Eqs. (16) and (17), this $\frac{\partial \phi}{\partial \bar{r}}$ -component, which is always pointed toward the jet axis, must be decomposed at the wing plane to produce the upwash. The x-induced velocity $\frac{\partial \phi}{\partial \bar{x}}$ is small in general and is neglected in the present applications.

3.3 An Equivalent Inviscid Jet in the Interaction Theory

As described in Appendix A, the velocity and temperature distributions in the turbulent jet vary not only in the axial direction but

also radially. The propagation of any disturbances in such a nonhomogeneous region would be governed by a partial differential equation win non-constant coefficients. To find a solution of such an equation would be difficult. To make the solution tractable, an equivalent homogeneous jet must be defined. In the present analysis, an equivalent jet with constant cross section and jet properties is assumed to be one which satisifes the conservation of mass, momentum and heat content and is evaluated at the midchord of the wing if the jet exit is ahead of the leading edge. The use of an equivalent jet in the wing-slipstream interaction problem has been shown to yield reasonably good results (Ref. 16). The detail of determining the equivalent jet properties is described in Appendix B.

Let $\tilde{r}_j$ be the equivalent jet radius. It is assumed that if the turbulent jet as defined in Appendix A intersects the wing surface and follows it to deflect at the trailing edge (to be discussed in more detail later), an upper-surface-blowing rectangular jet with lateral extent equal to $2\tilde{r}_j$ can be used for interaction computation. The main reason behind this assumption is that a jet washing the wing surface most likely has a cross section of half ellipse rather than a circle (Ref. 17). A rectangular jet would be most convenient to use. In this case, the situation would be that of upper-surface blowing, so that the theory of Ref. 11 can be directly used.

On the other hand, if the jet does not wash the wing, or if the jet is strong enough to go straight, the circular shape for the equivalent jet is retained. In the computation, the circular jet is in turn approximated by an inscribed polygon. This is shown in Fig. 1. To see how well this polygon can approximate the circle, a 2-D case is con-

structed. In the 2-D case, the exact solution can be obtained by Koning's image method(Ref. 18). According to the image method, a vortex of unit strength situated outside of the circular jet will induce, due to interaction, additional perturbation in the outside flow field which can be represented by an image vortex A of strength $-(s^2-1)/(s^2+1)$ at the inverse point and a vortex B of strength $(s^2-1)/(s^2+1)$ at the center, where $s=V_j/V_\infty$. This is described in Fig 2.

In the present model, two vortex sheets are used on the jet surface, as described in Section 3.1. Through numerical experimentation, it was found that one chord length of jet each ahead of the leading edge and behind the trailing edge would be sufficient for numerical convergence. Seven vortex elements for each streamwise vortex strip of the jet ahead of the leading edge and only one element for the jet behind the trailing edge were used, in order to reduce the computing time. It appeared that the trailing jet had negligible effect on the induced downwash near the leading edge. Therefore, in the following comparison, the additional induced downwash near the leading edge is plotted and compared with the results by the image method. This is done in Figs. 3(a) and 3(b) for two different originating vortex locations. As shown, the present approximation appears to be reasonably good. Further improvement of the accuracy seems to be limited by the accuracy of sidewash computation which is needed in calculating the induced normal velocity on the jet surface.

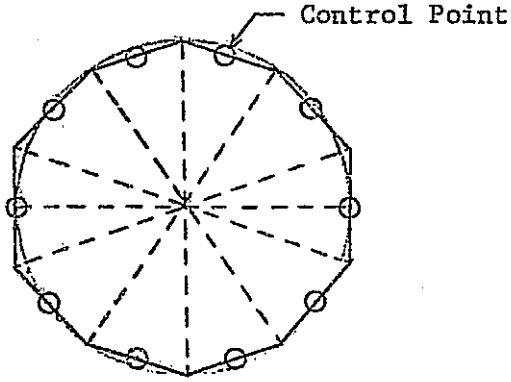

Figure 1 Geometric Approximation for a Circular Jet

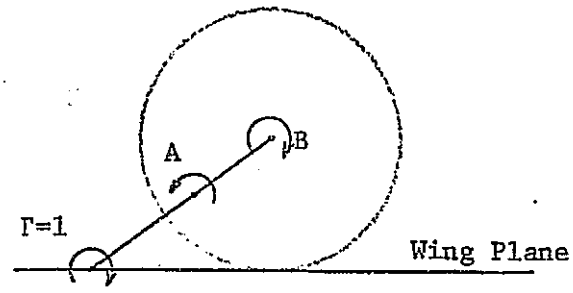

Figure 2 Image Method

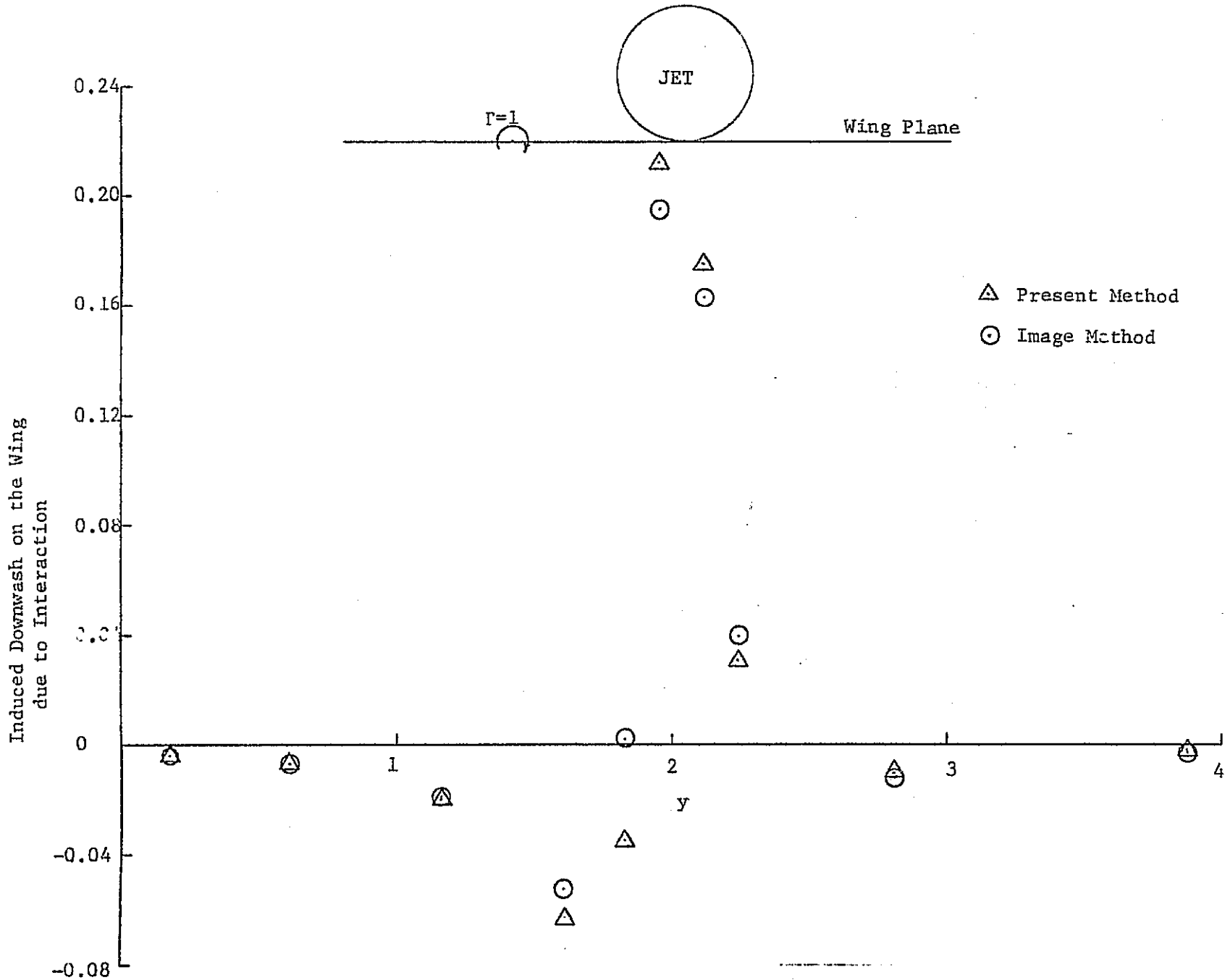

Figure 3Q Additional Induced Downwash as Predicted by the Present Method and the Image Method under 2-D Conditions

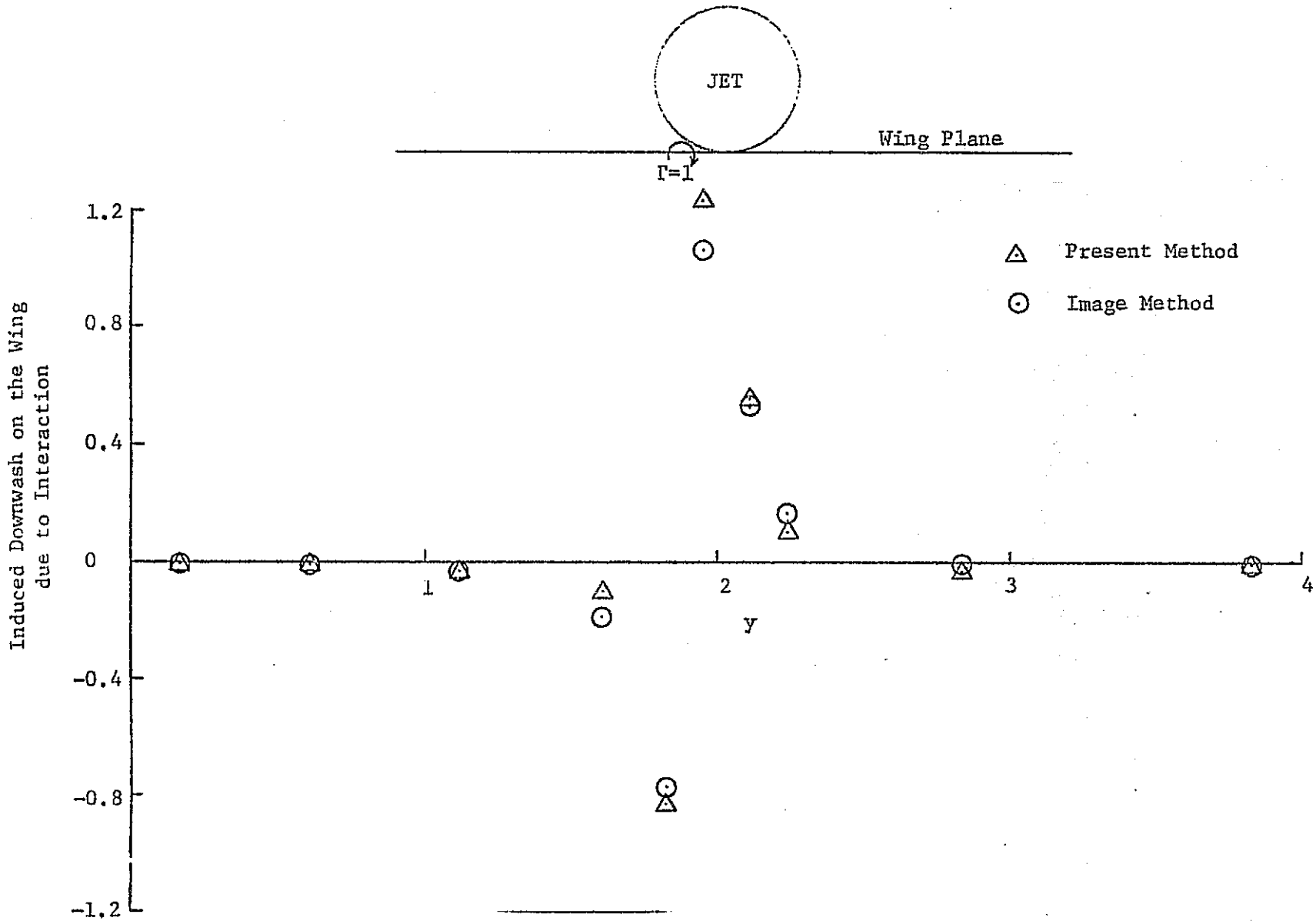

Figure 3b-Concluded

4. Numerical Results and Discussions

4.1 Some Observations of Falk's Experimental Data

For convenience, the jet-wing geometry parameters are defined in Fig. 4.

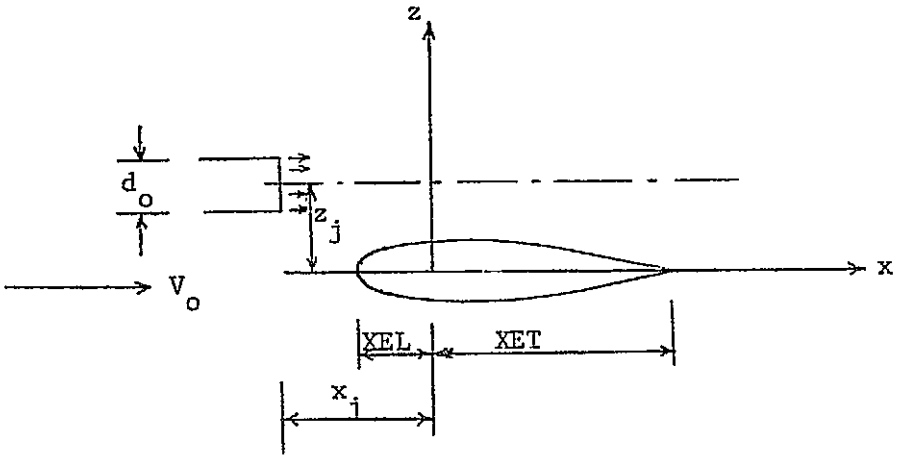

Figure 4 Wing-Jet Geometry

Before applying the above theory to any configurations, it is necessary to know what the jet deflection angle is when it washes the wing. The deflection would occur even if the flap angle is zero. This is because the jet has the tendency to follow the airfoil upper surface and leaves the trailing edge at an angle equal to or less than half the airfoil trailing-edge angle. However, since the jet is thick, its deflection will not be expected to be at full trailing edge angle at all times. Intuitively, at a given jet exit location, if the jet velocity is high relative to the freestream, the jet will have the tendency to go straight. Therefore, the deflection angle will be small. On the

other hand, the deflection angle will be larger if the jet axis is moved toward the wing surface. Furthermore, if the jet exit location is moved forward away from the leading edge, the measured lift seems to be increased according to Falk's data. This is illustrated in Figure 5. Theoretically, the jet entrainment would be lower near the wing region when the jet exit is farther away from the leading edge (i.e., $x_j/d_o = -6$). However, the measured lift increment is higher with $z_j/d_o \leq 1$. This seems to imply that the jet will deflect at a larger angle. In summary, the jet deflection angle for the thick jet under consideration is a function of μ, x_j/d_o and z_j. Without determining its correct variation, it would not be possible to predict the interaction effects. Since a theoretical analysis of this problem is beyond the scope of the present investigation, empirical relations would be useful alternatives. The effects of μ and x_j/d_o can be combined by using the equivalent velocity ratio $\bar{\mu}$ (i.e., $u_e/\tilde{u}_j$) defined in Appendix B. The following procedures are then used to derive such empirical relations.

(1) Three μ's (0.333, 0.4 and 0.5405) in Falk's experiments for a rectangular Wing of AR = 2 at $x_j/d_o = -1$ and $z_j/d_o = 1$ are used for correlation. The deflection angles are taken to be those which would produce the correct ΔC_L. If δ_e is the maximum possible deflection angle, then the actual jet deflection angle obtained through the above correlation using $\bar{\mu}$ computed at the wing midchord can be written as

$$\delta_j = f\,\delta_e \tag{42}$$

where

$$f = -29.5428\bar{\mu}^2 + 33.7371\bar{\mu} - 8.9148 \quad , \quad \bar{\mu} \leq 0.6339 \tag{43}$$

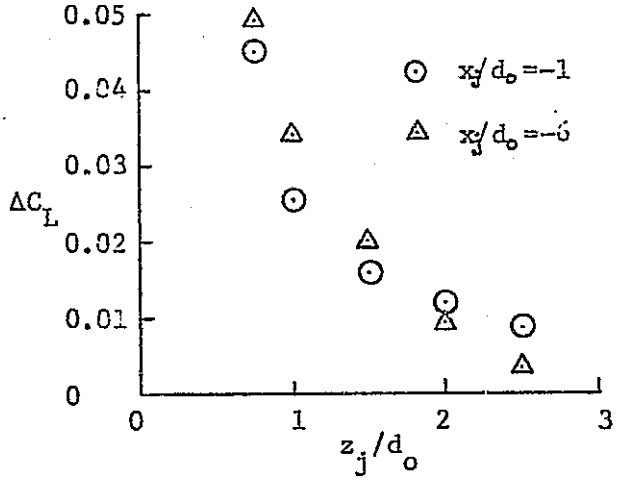

Figure 5 Effects of Jet Exit Locations on Falk's Experimental Lift Increments. $\mu=0.333$, $\alpha=0°$

where $\bar{\mu} = 0.6339$ is the equivalent velocity ratio for $\mu = 0.5405$. For $\bar{\mu} > 0.6339$, linear interpolation between f at $\bar{\mu} = 0.6339$ and f = 1 at $\bar{\mu} = 1$ is used. If f is negative by Eq. (43), f is to be replaced by zero and the equivalent jet is assumed to be circular, instead of a rectangular one.

(2) For $z_j/d_o \leq 0.75$, full deflection angle and rectangular jets are assumed irrespective of $\bar{\mu}$ values.

(3) Linear interpolation is used for $0.75 < z_j/d_o < 1.0$.

Further assumption is made that even if the jet is deflected, no jet reaction forces (i.e. Coanda forces) will be produced. This is based on the observation of static data which show that the lift force will

still be produced even if the jet is moved away from the wing. Therefore, the lift is not produced by jet reaction. Also, the fact that the jet tends to attach itself to the wing surface is mainly due to the jet entrainment, the effect of which has already been included. The static lift force may be explained as produced by the jet suction effect (or entrainment effect) which is called "Lagally force" in hydrodynamics (p. 215, Ref. 19). The Lagally force is neglected in the following applications.

4.2 Comparison of Predicted Results with Experiments

Falk's experiments represented an early investigation of over-wing-blowing aerodynamics. Systematic measurements of lift increments due to jet blowing have been made for different jet exit locations varied both vertically and horizontally. For his rectangular wing of AR = 2, which will be used in the following comparison, the airfoil section was a symmetric modified Joukowski airfoil of 16% thickness ratio. By "modified," it is interpreted here as a Joukowski airfoil with straightened trailing edge by drawing tangents to the surface from the trailing edge, instead of the usual cusped shape. The trailing edge half angle can therefore be obtained in the following way. According to Glauert (p. 75 of Ref. 31), the symmetric Joukowski airfoils can be approximately represented by the following equations:

$$x = \frac{c}{2}\cos\theta \tag{44a}$$

$$y = \frac{c}{2}\frac{4}{3\sqrt{3}}\left(\frac{t}{c}\right)(1+\cos\theta)\sin\theta \tag{44b}$$

where c is the chord length. The slope is therefore given by

$$m' = \frac{dy}{dx} = -\frac{\frac{4}{3\sqrt{3}}\left(\frac{t}{c}\right)\left[-\sin^2\theta + \cos\theta + \cos^2\theta\right]}{\sin\theta} \tag{45}$$

The trailing edge is at x = -c/2. The equation for the straight line which passes through the trailing edge and is tangent to the airfoil is then

$$y = m'\left(x + \frac{c}{2}\right) \tag{46}$$

The tangent point location θ_1 can be obtained from the following equation:

$$\frac{c}{2}\cdot\frac{4}{3\sqrt{3}}\left(\frac{t}{c}\right)(1+\cos\theta_1)\sin\theta_1 = -\frac{\frac{4}{3\sqrt{3}}\left(\frac{t}{c}\right)\left[-\sin^2\theta_1 + \cos\theta_1 + \cos^2\theta_1\right]}{\sin\theta_1}\left(\frac{c}{2}\cos\theta_1 + \frac{c}{2}\right)$$

from which $\cos\theta_1 = \frac{2}{3}$. Hence, m' = -0.0918 from Eq. (45) for t/c = 0.16. It follows that $\delta_e = 5.25°$.

The predicted results for 3 μ's at two different jet exit x-locations are compared with Falk's experiments in Figure 6. From this comparison, the following points should be noted. Firstly, the present theory with entrainment alone agrees very well with Putnam's calculation for μ = 0.333 and x_j/d_o = -1. However, the entrainment-alone theory tends to underestimate the lift for $z_j/d_o \leq 1.5$, as has been noted by Putnam (Ref. 9). Secondly, for $z_j/d_o \leq 1.5$, the present results with both interaction effects and entrainment agrees reasonably well with experiments. For μ = 0.25, x_j/d_o = -1 and z_j/d_o = 0.75, the prediction appears to be too high, probably because it was assumed that the jet was deflected at the full trailing-edge half angle. Thirdly, as the nacelle is raised upwards, the theoretical method tends to overpredict the lift, even without interaction effects. One possible explanation is that the wing might have been affected by the low dynamic-pressure viscous layer from the nacelle which is ahead of the leading edge. Such effect has been noted by Stüper in his experiments on wing-slipstream interaction [Ref. 32].

To test the theory with compressibility effect, Putnam's experiments on a swept wing with the engine pressure ratio of 1.9 are compared. The

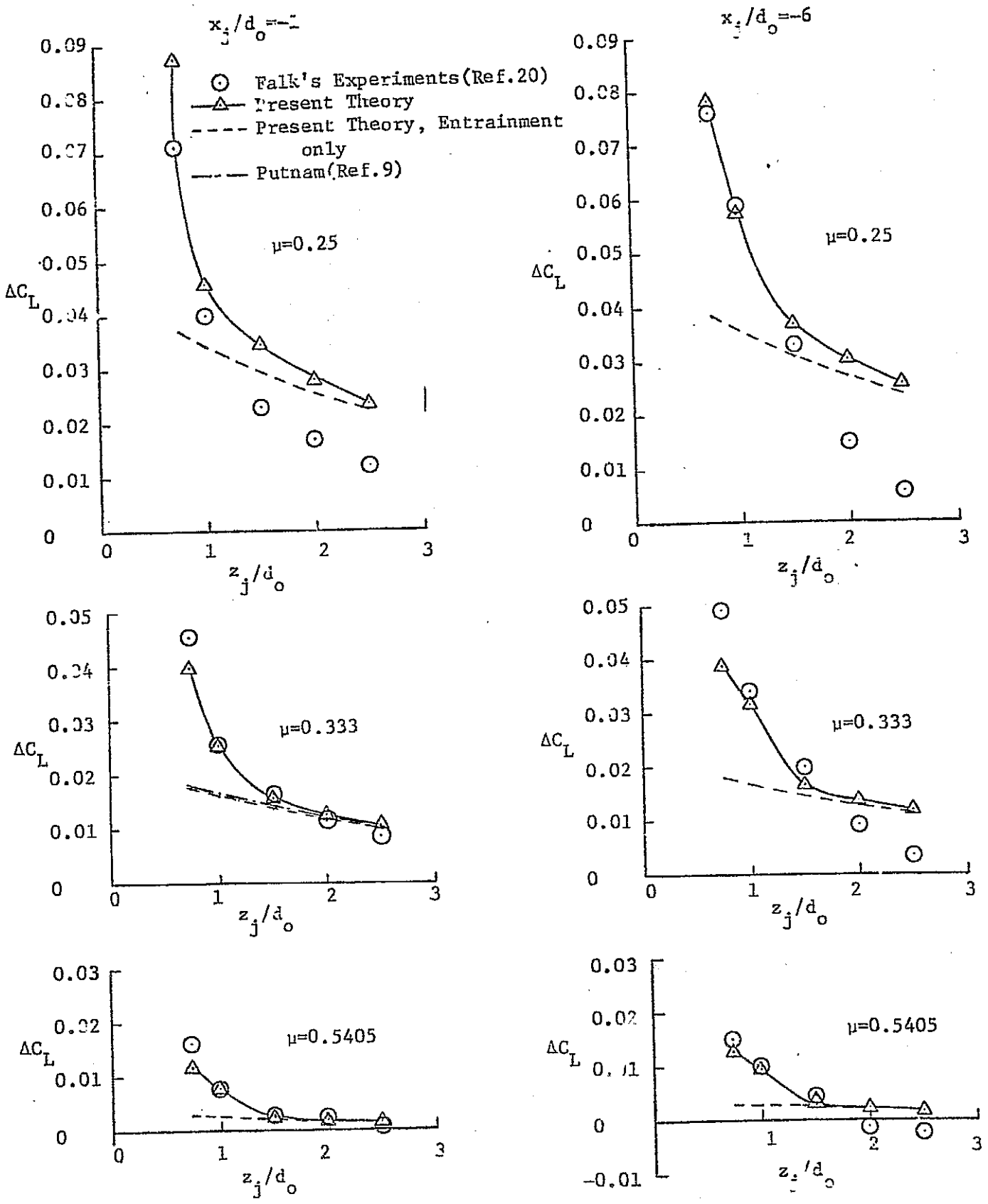

Figure 6 Comparison of Predicted Results with Falk's Experiments. M_∞=0, M_j=0 and α=0°

experimental data are shown on Figure 18 of Ref. 5. Since the velocity ratio, temperature ratio and the jet Mach number are needed, they will be computed in accordance with isentropic relations. (See Chapter 2 of Ref. 33):

$$M_j^2 = \frac{2}{\gamma-1}\left[\left(\frac{p_{t,j}}{p_\infty}\right)^{\frac{\gamma-1}{\gamma}} - 1\right] \tag{47}$$

$$\frac{T_{t,j}}{T_j} = 1 + \frac{\gamma-1}{2} M_j^2 \tag{48}$$

$$\frac{T_{t,\infty}}{T_\infty} = 1 + \frac{\gamma-1}{2} M_\infty^2 \tag{49}$$

If the jet is not heated, it may be assumed that $T_{t,j} = T_{t,\infty}$. It follows that at the jet exit,

$$\frac{T_j}{T_\infty} = \frac{\rho_\infty}{\rho_j} = \frac{1 + \frac{\gamma-1}{2} M_\infty^2}{1 + \frac{\gamma-1}{2} M_j^2} \tag{50}$$

$$\frac{V_\infty}{V_j} = \mu = \frac{M_\infty}{M_j} \Big/ \sqrt{\frac{T_j}{T_\infty}} \tag{51}$$

Using the above relations, it is found that for $p_{t,j}/p_\infty = 1.9$, $M_j = 1.003$, $\rho_\infty / \rho_j = 0.85914$ and $\mu = 0.43026$. Note that $M_j > 1$ is allowed in the entrainment computation. In the interaction computation, the jet Mach number used in the program is given by

$$\tilde{M}_j = M_\infty \left(\frac{\tilde{u}_j}{u_e}\right)\left(\frac{\tilde{\rho}_j}{\rho_e}\right)^{1/2} \tag{52}$$

where $\tilde{u}_j$ and $\tilde{\rho}_j$ are equivalent values evaluated at midchord. The equivalent jet Mach number will be much less that one in the present application. The trailing-edge half angle for NACA64A006 airfoil used in the experiments is found to be 3.6°. The results are shown in Figure 7. The agreement with experiments is good.

Finally, Seidel's experiments will be examined and compared. In his test set-up, the jet exit was at least one chord length ahead of the leading-edge. Since the test speed was low, the freestream and jet Mach

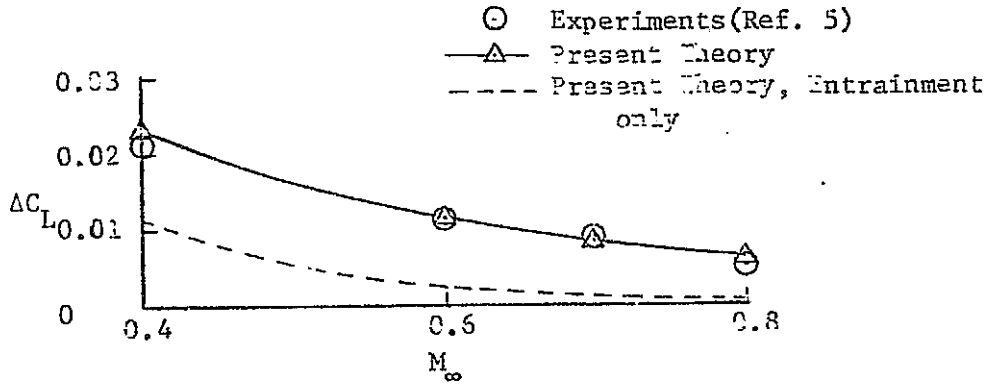

Figure 7 Comparison of Predicted Results with Putnam's Experiments. z_j/d_o= 0.75, $p_{t,j}/p_\infty$=1.9 and α=0°

numbers can be assumed to be zero. The trailing-edge half angle for NACA 0010 is found to be 6.67°. The predicted results are compared with the measured data in Figure 8. The computed magnitude of ΔC_L is slightly lower than the measurement probably because part of the wing may be immersed in the jet as indicated by the present turbulent jet theory. When part of the wing is immersed in the jet, the wing-slipstream interaction theory (Ref. 34) should be used. However, this has not been done in the present preliminary investigation.

5. Conclusions

A theoretical method has been described for determining the aerodynamic characteristics of over-wing-blowing configurations. The method accounts for not only the jet entrainment but also the jet interaction effects due to the differences in freestream and jet dynamic pressures and Mach numbers. The jet entrainment is determined by a new method which is an extension of Kleinstein's free turbulent jet theory. Comparison of the theoretical results with some available data indicates

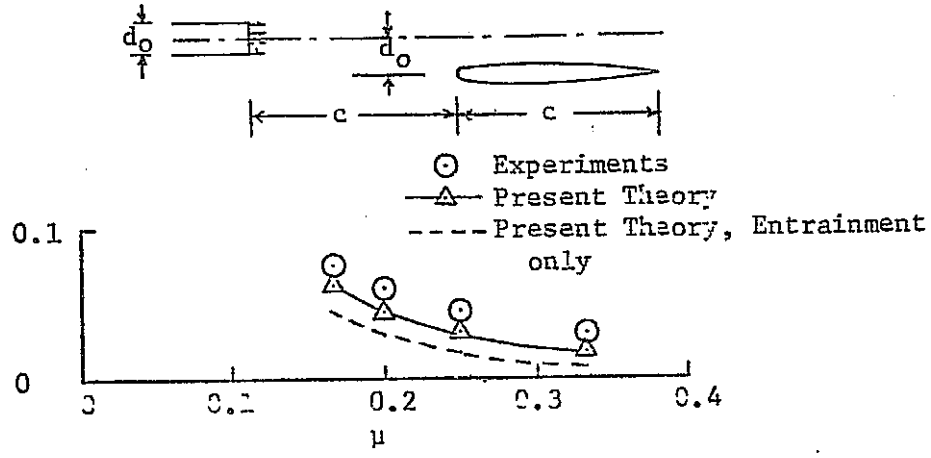

Figure 8 Comparison of Predicted Results with Seidel's Experiments. $M_\infty=0$, $M_j=0$, $z_j/d_o=1$ and $\alpha=0°$

reasonably good agreement. From the examination of some experimental data and the theoretical entrainment function, it appears that the entrainment-induced lift can be maximized by placing the wing in the region of maximum entrainment. However, any favorable wing-jet interaction including the jet flap effect should also be examined for an optimum engine location.

6. References

(1.) Bagley, J.A., "Some Experiments on an Engine Installation Above the Wing of a Swept-Winged Aircraft", Preceedings of the DGLR Symposium on Aerodymanic Interference between Aircraft and Engine Jet, Dec. 3, 1970

(2.) Kettle, D.J., Kurn, A.G. and Bagley, J.A., "Exploratory Tests on a Forward-Mounted Overwing Engine Installation", Aeronautical Research Council of Great Britain, C.P. No. 1207, 1972

(3.) "Airframe-Engine Interaction for Engine Configurations Mounted above the Wing", AGARD CP-150, Airframe/Propulsion Interference, September 1974.

Part 1. Interference between Wing and Intake/ Jet, by G. Krenz

Part 2. Engine Jet Simulation Problems in Wind Tunnel Tests, by B. Ewald

(4.) Seidel, M., "The Influence of an Inclined Jet on the Flow Field in the Vicinity of a Lifting Surface and on Its Aerodynamic Coeffieients", NASA TT F-14956, July 1973

(5.) Putnam, Lawrence E., "Exploratory Investigation at Mach Numbers from 0.40 to 0.95 of the Effects of Jets Blown over a Wing," NASA TN D-7367, Nov. 1973

(6.) Squire, H.B. and Trouncer, J., "Round Jets in a General Stream", Aeronautical Research Council of Great Britain, R&M No. 1974 Jan. 1944

(7.) Squire, H.B., "Jet Flow and Its Effects on Aircraft", Aircraft Engineering, Vol. 22, 1950, pp. 62-67.

(8.) Ribner, H.S. , "Field of Flow about a Jet and Effect of Jets on Stability of Jet-Propelled Airplanes", NACA ACR No. L6C13 April 1946

(9.) Putnam, Lawrence E., "An Analytical Study of the Effects of Jets Located More Than One Jet Diameter Above a Wing at Subsonic Speeds", NASA TN D-7754. Aug. 1974

(10.) Kleinstein, G., "Mixing in Turbulent Axially Symmetric Free Jets", Journal of Spacecraft and Rockets, Vol. 1, No. 4, July-Aug. 1964, pp. 403-408

(11.) Lan, C.Edward and Campbell, James F., " Theoretical Aerodynamics of Upper-Surface-Blowing Jet-Wing Interaction", NASA TN D-7936, Nov. 1975

(12.) Lan, C. Edward, "Some Characteristics of Airfoil-Jet Interaction with Mach Number Nonuniformity", Journal of Aircraft, Vol.11 No. 8, Aug. 1974, pp. 491-494.

(13.) Lan, C.E., "A Quasi Vortex-Lattice Method in Thin Wing Theory", Journal of Aircraft, Vol. 11, No. 9, Sept. 1974, pp. 518-527

(14.) Fox, H., Sinha, R. and Weinberger, L., "An Implicit Finite Difference Solution for Jet and Wake Problems", Astronautica Acta, Vol 17, No. 3, 1972, pp. 265-278.

(15.) Sears, W.R., "Small Perturbation Theory" in General Theory of High Speed Aerodynamics, Princeton Series Vol. 6, 1954

(16.) Kleinstein, G. and Liu, C.H., "Application of Airfoil Theory for Nonuniform Streams to Wing Propeller Interaction", Journal of Aircraft, Vol. 9, No. 2, Feb. 1972, pp. 137-142

(17.) Newman, B.G., Patel, R.P., Savage, S.B. and Tjio, H.K., "Three-Dimensional Wall Jet Originating from a Circular Orifice", Aeronautical Quarterly, Vol. 23, Part 3, August 1972, pp. 188-200

(18.) Koning, C., "Influence of the Propeller on Other Parts of the Airplane Structure", in Vol. IV of "Aerodynamic Theory", Ed. by W.F. Durand; Dover Publication

(19.) Milne-Thomson, L.M. "Theoretical Hydrodynamics", 4th Edition, 1962, MacMillan Co.

(20.) Falk, H., "The Influence of the Jet of a Propulsion Unit on Nearby Wings", NACA TM 1104, 1946

(21.) Abramovich, G.N., "The Theory of Turbulent Jets", MIT Press, 1963

(22.) Shanks, D., "Non-linear Transformations of Divergent and Slowly Convergent Sequences", Journal of Mathematics and Physics, Vol. 34, 1955, pp. 1-42

(23.) Ricou, F.P. and Spalding, D.B., "Measurements of Entrainment by Axisymmetrical Turbulent Jets", Journal of Fluid Mechanics, Vol. 11, Aug.-Dec., 1961, pp. 21-32

(24.) Hill,B.J., "Measurement of Local Entrainment Rate in the Initial Region of Axisymmetrical Turbulent Air Jets", Journal of Fluid Mechanics, Vol. 51, Pt. 4, 1972, pp. 773-779

(25.) Boyle, R.E. Jr. and Viets, H., "Eddy Viscosity for Variable Density Coflowing Stream", ARL 73-0172, Aerospace Research Laboratories of the Air Force. Also, Journal of Aircraft, Vol. 11, No. 12, Dec. 1974,pp. 721-722

(26.) Schetz, J.A., "Unified Analysis of Turbulent Jet Mixing", NASA CR-1382, July 1969

(27.) Witze, P.O., "Centerline Velocity Decay of Compressible Free Jets", AIAA Journal, Vol. 12, No. 4, Apr. 1974, pp. 417-418

(28.) Gentry, C.L. and Margason, R.J., "Jet-Induced Lift Losses on VTOL Configurations Hovering in and out of Ground Effect", NASA TN D-3166, Feb. 1966

(29.) Wygnanski, I., "The Flow Induced by Two-Dimensional and Axi-symmetric Turbulent Jets Issuing Normally from an Infinite Plane Surface", The Aeronautical Quarterly, Vol. 15, Pt. 4, Nov. 1964, pp.370-380

(30.) Skifstad, J.G., "Aerodynamics of Jets Pertinent to VTOL Aircraft", Journal of Aircraft, Vol. 7, No. 3, May-June 1970, pp. 193-204

(31.) Glauert, H., "The Elements of Aerofoil and Airscrew Theory", Cambridge University Press, 1959

(32.) Stüper, J., "Effect of Propeller Slipstream on Wing and Tail", NACA TM 874, August 1938

(33.) Liepmann,H.W. and Roshko, A., "Elements of Gasdynamics", John Wiley & Sons, Inc. 1963

(34.) Lan, C. Edward, "Wing-Slipstream Interaction with Mach Number Nonuniformity", Journal of Aircraft, Vol. 12, No. 10, October 1975, pp. 759-760

Appendix A

An Extension of Kleinstein's Compressible Turbulent Jet Theory to the Computation of Jet Entrainment

A.1. Turbulent Jet Model

The momentum integral relation for the jet can be written as

$$\int_0^{r_j} \rho u r (u - u_e)\, dr = M = \frac{r_o^2}{2} \rho_j u_j (u_j - u_e) \qquad (A.1)$$

where r_j is the radius of the jet boundary and r_o is the jet radius at the exit. For the fully developed region, it may be assumed that (Ref. 21, p. 306)

$$u = u_e + (u_c - u_e)(1 - \xi_1^{3/2})^2 \qquad (A.2)$$

$$T = T_e + (T_c - T_e)(1 - \xi_1^{3/2}) \qquad (A.3)$$

$$\xi_1 = r/r_j \qquad (A.4)$$

Define the nondimensional variables:

$$\bar{\rho} = \rho/\rho_j \;,\; \bar{u} = u/u_j \;,\; \bar{u}_e = \mu = u_e/u_j \qquad (A.5)$$

It follows that Eq. (A.2) can be written as

$$\bar{u} = \mu + (\bar{u}_c - \mu)(1 - \xi_1^{3/2})^2 \qquad (A.6)$$

Assuming constant pressure mixing, the density can then be written as

$$\bar{\rho} = \frac{R_j T_j}{R T} = \frac{T_j R_j}{T_e R} \frac{1}{1 + (\frac{T_c}{T_e} - 1)(1 - \xi_1^{3/2})} \qquad (A.7)$$

where R_j and R are the gas constants of the exit jet and the jet-air mixture, respectively. It follows that Eq. (A.1) can be reduced to

$$\rho_j u_j^2 r_j^2 \int_0^1 \bar{\rho}\, \bar{u}\, \xi_1 (\bar{u} - \mu)\, d\xi_1 = M$$

$$= \rho_j u_j^2 r_j^2 \frac{T_j R_j}{T_e \bar{R}} \int_0^1 \frac{\mu + (\bar{u}_c - \mu)(1 - \xi_1^{3/2})^2}{1 + (\frac{T_c}{T_e} - 1)(1 - \xi_1^{3/2})} \xi_1 (\bar{u}_c - \mu)(1 - \xi_1^{3/2})^2\, d\xi_1 \qquad (A.8)$$

where $\bar{R}$ is the average gas constant for the mixture.

The integrals invovled in Eq. (A.8) can be integrated exactly. However, the results are difficult to evaluate numerically when $\frac{T_c}{T_e} - 1$ is small. Since $(\frac{T_c}{T_e} - 1)$ is, in general, not large in the fully-developed region, it is convenient to develop the integrand in a

power series with respect to $(\frac{T_c}{T_e} - 1)$ and integrate the results exactly. In order to accelerate the series convergence, Shanks' Transformation (Ref. 22) can be used. When the above-mentioned process is applied to Eq. (A.8), it is obtained that (see Appendix C for one example)

$$S_j u_j^2 r_j^2 \frac{T_j R_j}{T_e \bar{R}} (P_1 \mu F_1 + P_1^2 F_2) = M \tag{A.9}$$

where

$$P_1(x) = \bar{u}_c(x) - \mu \tag{A.10}$$

$$F_1 = \int_0^1 \frac{\xi_1 (1-\xi_1^{3/2})^2}{1 + P_2 (1-\xi_1^{3/2})} d\xi_1$$

$$\simeq \frac{0.12857 + 0.01617 P_2 - 0.00607 P_2^2 + 0.00192 P_2^3}{1 + 0.81817 P_2} \tag{A.11}$$

$$F_2 = \int_0^1 \frac{\xi_1 (1-\xi_1^{3/2})^4}{1 + P_2 (1-\xi_1^{3/2})} d\xi_1$$

$$\simeq \frac{0.06676 + 0.00453 P_2 - 0.00204 P_2^2 + 0.00075 P_2^3}{1 + 0.85716 P_2} \tag{A.12}$$

$$P_2(x) = \frac{T_c(x)}{T_e} - 1 \tag{A.13}$$

Eq. (A.9) gives a relation between the jet radius r_j and the axial flow properties. Here, the axial flow properties will be obtained by an extension of Kleinstein's theory (Ref. 10).

Extension of Kleinstein's theory

Kleinstein's theory is based on the linearization of the jet flow equations on von Mises' plane. The longitudinal velocity $\bar{u} = u/u_j$ at any x is expressed in terms of the P-function as

$$\bar{u} = \mu + (1-\mu) P_o P^*(\sqrt{2}/(2\xi)^{1/2}, \psi/(2\xi)^{1/2}) \tag{A.14}$$

where P* is the normalized P-function and P_o is related to $\bar{u}_c$ by

$$\bar{u}_c = \mu + (1-\mu) P_o \tag{A.15}$$

$$P_o = 1 - \exp(-1/2\xi) \tag{A.16}$$

The ξ - variable is related to $\bar{x} = x/r_o$ by

$$\frac{d\xi}{d\bar{x}} = 2\,\overline{\rho\varepsilon} \tag{A.17}$$

where $\overline{\rho\varepsilon}$ is the non-dimensional turbulent transfer coefficient.

The relation between ψ, the stream function, and the radial coordinate $\bar{r}$ is given by

$$\bar{r}^2 = \int_0^{\psi} \frac{\psi\, d\psi}{\bar{\rho}\,\bar{u}} \tag{A.18}$$

where

$$\bar{r} = r/r_o \tag{A.19}$$

According to Ferri's turbulent eddy viscosity model, $\overline{\rho\varepsilon}$ in the fully developed region can be assumed to be

$$\overline{\rho\varepsilon} = k_1\, \bar{b}_{1/2}\,(\bar{\rho}_c\,\bar{u}_c - \bar{\rho}_e\,\mu) \tag{A.20}$$

where $\bar{b}_{1/2}$ is the raidus at which the flow properties satisfy

$$\bar{\rho}\bar{u} = \frac{1}{2}(\bar{\rho}_c\,\bar{u}_c + \bar{\rho}_e\,\mu) \quad , \quad \bar{r} = \bar{b}_{1/2} \,. \tag{A.21}$$

To use the above expressions, consider the asymptotic expansions for $\xi \to \infty$, i.e., far downstream. In this region, $\bar{\rho} \to \bar{\rho}_e$ and $\bar{\rho}_c \to \bar{\rho}_e$. Hence, Eq. (A.21) becomes

$$\bar{u} = \frac{1}{2}(\mu + \bar{u}_c) \quad , \quad \bar{r} = \bar{b}_{1/2} \,.$$

From Eq. (A.14)

$$\mu + (1-\mu)\,P_o\,P^*\left(\frac{\sqrt{2}}{\sqrt{2\xi}}\,,\frac{\psi_{1/2}}{\sqrt{2\xi}}\right) = \frac{1}{2}[\mu + \mu + (1-\mu)P_o]$$

or,

$$P_o\,P^*\left(\frac{\sqrt{2}}{\sqrt{2\xi}}\,,\frac{\psi_{1/2}}{\sqrt{2\xi}}\right) = \frac{1}{2}P_o \tag{A.22}$$

Now, $P^*\left(\frac{\sqrt{2}}{\sqrt{2\xi}}\,,\frac{\psi}{\sqrt{2\xi}}\right) \xrightarrow[\xi\to\infty]{} e^{-\psi^2/4\xi}$ and $P_o \longrightarrow \frac{1}{2\xi}$. Hence,

$$\bar{b}_{1/2}^2 = \int_0^{\psi_{1/2}} \frac{\psi\, d\psi}{\bar{\rho}\,\bar{u}} = \frac{1}{\bar{\rho}_e}\int_0^{\psi_{1/2}} \frac{\psi\, d\psi}{\mu + (1-\mu)P_o P^*} = \frac{1}{\bar{\rho}_e}\int_0^{\psi_{1/2}} \frac{\psi\, d\psi}{\mu + (1-\mu)P_o\, e^{-\psi^2/4\xi}}$$

$$= \frac{1}{\bar{\rho}_e}\int_0^{\psi_{1/2}} \frac{e^{\frac{\psi^2}{4\xi}}\,\psi\, d\psi}{\mu e^{\psi^2/4\xi} + (1-\mu)P_o} = \frac{4\xi}{2\bar{\rho}_e\mu}\,\ln\frac{1 + \frac{\mu}{(1-\mu)P_o}\,e^{\psi_{1/2}^2/4\xi}}{1 + \frac{\mu}{(1-\mu)P_o}}$$

But

$$P_0 P^*\left(\frac{\sqrt{2}}{\sqrt{2\xi}}, \frac{\psi_{1/2}}{\sqrt{2\xi}}\right) \longrightarrow P_0 e^{-\psi_{1/2}^2/4\xi} \rightarrow \frac{1}{2}\frac{1}{2\xi} \quad , \quad P_0 \rightarrow \frac{1}{2\xi}$$

by Eq. (A.22). Hence

$$\bar{b}_{1/2}^2 = \frac{2\xi}{\bar{S}_e \mu} \ln \frac{1+\frac{\mu}{1-\mu}4\xi}{1+\frac{\mu}{1-\mu}2\xi} \quad . \tag{A.23}$$

Using Eq. (A.15), Eq. (A.20) can be written as, when $\xi \rightarrow \infty$,

$$\bar{S}\bar{\varepsilon} \longrightarrow k_1 \sqrt{\frac{2\xi}{\bar{S}_e \mu}} \left[\ln \frac{1+\frac{\mu}{1-\mu}4\xi}{1+\frac{\mu}{1-\mu}2\xi}\right]^{1/2} \bar{S}_e (1-\mu)\frac{1}{2\xi}$$

$$= \frac{k_1 \sqrt{\bar{S}_e}}{\sqrt{2\mu\xi}} (1-\mu)\left[\ln \frac{1+\frac{\mu}{1-\mu}4\xi}{1+\frac{\mu}{1-\mu}2\xi}\right]^{1/2} \tag{A.24}$$

Eq. (A.24) is valid only far downstream. To extrapolate this result to the near field, it is most convenient to use $P_0(\xi)$. That is, $\frac{1}{2\xi}$ in Eq. (A.24) is to be replaced by P_0. According to Eqs. (A.10) and (A.15), $P_1(\xi) = \bar{u}_c - \mu = (1-\mu)P_0$. It follows that $(1-\mu)\frac{1}{2\xi}$ in Eq. (A.24) is to be replaced by $P_1(\xi)$. Hence,

$$\bar{S}\bar{\varepsilon} = k_1 \sqrt{\bar{S}_e} \sqrt{\frac{1-\mu}{\mu}} \sqrt{P_1} \left[\ln \frac{1+\frac{2\mu}{P_1}}{1+\frac{\mu}{P_1}}\right]^{1/2} \tag{A.25}$$

For $\mu = 0$, Eq. (A.25) is reduced to Kleinstein's results for free jets:

$$\bar{S}\bar{\varepsilon} = k_1 \sqrt{\bar{S}_e} \quad , \mu = 0 .$$

Integrating Eq. (A.17), a relation between ξ and $\bar{x}$ can be obtained:

$$2k_1 \sqrt{\bar{S}_e} \sqrt{1-\mu}\, \bar{x} = \int_0^{\xi} \sqrt{\mu} \frac{d\xi}{\sqrt{P_1(\xi)}\sqrt{\ln \frac{1+\frac{2\mu}{P_1(\xi)}}{1+\frac{\mu}{P_1(\xi)}}}} + C_1 \tag{A.26}$$

$$P_1(\xi) = (1-\mu)P_0(\xi) = (1-\mu)\left[1 - e^{-\frac{1}{2\xi}}\right] = \bar{u}_c - \mu \tag{A.26a}$$

For $\mu = 0$, Eq. (A.26) gives

$$2k_1 \sqrt{\bar{S}_e}\, \bar{x} = \xi + C_1$$

Comparing this equation with Kleinstein's, it is obtained that $C_1 = 0.35$ which was obtained from experimental correlation.

The constant k_1 will be chosen later for correlation with experimental data. Eq. (A.26) may be regarded as a nonlinear algebraic equation for $\xi_j(\bar{x})$. For a given $\bar{x}$, the corresponding ξ_j, and therefore $\bar{u}_c$, can be obtained by Newton's method. Eq. (A.26) also shows that the potential core length is given by

$$\bar{x}_c = \frac{C_1}{2k_1\sqrt{\bar{S}_e}\sqrt{1-\mu}} = \frac{0.35}{2k_1\sqrt{\bar{S}_e}\sqrt{1-\mu}} \tag{A.27}$$

The integral involved in Eq. (A.26) can be evaluated as follows. For large ξ_j, the integrand becomes $\sqrt{2\mu\xi}/\sqrt{(1-\mu)\ln 2}$. Hence,

$$\sqrt{\mu}\int_0^{\xi_j}\frac{d\xi_1}{\sqrt{P_1}\sqrt{\ln\frac{1+\frac{2\mu}{P_1}}{1+\frac{\mu}{P_1}}}} = \sqrt{\mu}\int_0^{\xi_j}\left[\frac{1}{\sqrt{P_1}\sqrt{\ln\frac{1+\frac{2\mu}{P_1}}{1+\frac{\mu}{P_1}}}} - \sqrt{\frac{2\xi}{1-\mu}}\frac{1}{\sqrt{\ln 2}}\right]d\xi_j + \sqrt{\mu}\int_0^{\xi_j}\sqrt{\frac{2\xi}{(1-\mu)\ln 2}}\,d\xi_j$$

$$\cong \sqrt{\mu}\,\frac{1}{2}\xi_j\frac{\pi}{N}\sum_{k=1}^{N}\left[\frac{1}{\sqrt{P_{1k}}\sqrt{\ln\frac{1+\frac{2\mu}{P_{1k}}}{1+\frac{\mu}{P_{1k}}}}} - \sqrt{\frac{2\xi_{jk}}{1-\mu}}\frac{1}{\sqrt{\ln 2}}\right]\sin\theta_k + \sqrt{\frac{2\mu}{1-\mu}}\frac{2}{3}\frac{\xi_j^{3/2}}{\sqrt{\ln 2}} \tag{A.28}$$

where

$$\xi_{jk} = \frac{1}{2}\xi_j(1-\cos\theta_k), \quad \theta_k = \frac{2k-1}{2N}\pi \tag{A.29}$$

To complete the evaluation of flow properties on the jet axis, it is necessary to determine T_c. According to Kleinstein's theory, the stagnation enthalpy on the axis is given by

$$\frac{H_c - H_e}{H_j - H_e} = H_0(\xi_R) = 1 - e^{-\frac{1}{2\xi_R}} \tag{A.30}$$

$$\frac{d\xi_R}{d\bar{x}} = 2\frac{\bar{S}\bar{\varepsilon}}{P_r} \tag{A.31}$$

where P_r is the turbulent Prandtl number. From Eq. (A.31), it is seen that Eq. (A.26) can be modified to give

$$2\frac{k_1}{P_r}\sqrt{\bar{S}_e}\sqrt{1-\mu}\,\bar{x} = \int_0^{\xi_R}\sqrt{\mu}\,\frac{d\xi}{\sqrt{P_1(\xi)}\sqrt{\ln\frac{1+\frac{2\mu}{P_1(\xi)}}{1+\frac{\mu}{P_1(\xi)}}}} + 0.35 \tag{A.32}$$

Once H_0 is obtained, T_c can be obtained from the definition of the stagnation enthalpy:

$$H = C_p T + \frac{1}{2}u^2 \tag{A.33}$$

It follows that

$$\frac{H_c - H_e}{H_j - H_e} = H_o = \frac{C_p T_c + \frac{1}{2}u_c^2 - (C_p T_e + \frac{1}{2}u_e^2)}{C_p T_j + \frac{1}{2}u_j^2 - (C_p T_e + \frac{1}{2}u_e^2)}$$

$$= \frac{C_p(T_c - T_e) + \frac{1}{2}(u_c - u_e)(u_c + u_e)}{C_p(T_j - T_e) + \frac{1}{2}(u_j - u_e)(u_j + u_e)}$$

$$= \frac{\frac{C_p T_e}{u_j^2}\left(\frac{T_c}{T_e} - 1\right) + \frac{1}{2}P_1(\xi)[P_1(\xi) + 2\mu]}{\frac{C_p T_e}{u_j^2}\left(\frac{T_j}{T_e} - 1\right) + \frac{1}{2}(1-\mu^2)}$$

But

$$\frac{C_p T_e}{u_j^2} = \frac{T_e}{(\gamma-1)M_j^2 T_j},$$

where M_j is the jet Mach number. It follows that

$$H_o = \frac{\frac{1}{(\gamma-1)M_j\theta}\left(\frac{T_c}{T_e} - 1\right) + \frac{1}{2}P_1[P_1 + 2\mu]}{\frac{1}{(\gamma-1)M_j^2\theta}(\theta - 1) + \frac{1}{2}(1-\mu^2)}, \quad \theta = \frac{T_j}{T_e}.$$

Solving for T_c/T_e, it is found that

$$\frac{T_c}{T_e} - 1 = P_2(\xi) = [\theta - 1 + \frac{\gamma-1}{2}(1-\mu^2)M_j^2\theta]H_o - \frac{\gamma-1}{2}M_j^2\theta P_1[P_1 + 2\mu] \quad (A.34)$$

A.2. Entrainment

$$m = 2\pi\int_o^r \rho u r\,dr, \quad r > r_j$$

$$= 2\pi\left\{\int_o^{r_j} \rho u r\,dr + \int_{r_j}^r \rho_e u_e r\,dr\right\}$$

$$= 2\pi\left\{\int_o^{r_j} \rho u r\,dr + \frac{1}{2}\rho_e u_e r^2 - \frac{1}{2}\rho_e u_e r_j^2\right\}$$

$$= 2\pi\left\{\int_o^{r_j} (\rho u - \rho_e u_e) r\,dr + \frac{1}{2}\rho_e u_e r^2\right\} \quad (A.35)$$

The entrainment is the increase in the mass flow rate per unit distance.

Hence,

$$\frac{\partial m}{\partial x} = \text{Entrainment} = 2\pi\frac{\partial}{\partial x}\int_o^{r_j} (\rho u - \rho_e u_e) r\,dr \quad (A.36)$$

Let

$$J = \int_o^{r_j} (\rho u - \rho_e u_e) r\,dr = \rho_j u_j r_j^2 \int_o^1 (\bar{\rho}\bar{u} - \bar{\rho}_e \mu)\xi_1\,d\xi_1$$

$$= \rho_j u_j r_j^2 \frac{T_j R_j}{T_e \bar{R}} \int_o^1 \left[\frac{\mu + (\bar{u}_c - \mu)(1-\xi_1^{3/2})^2}{1 + (\frac{T_c}{T_e} - 1)(1-\xi_1^{3/2})} - \mu\right]\xi_1\,d\xi_1$$

$$= \rho_j u_j r_j^2 \frac{T_j R_j}{T_e \bar{R}}[P_1 F_1 - \mu P_2 F_3] \quad (A.37)$$

where $\bar{R}$ is the average gas constant for the mixture and may be assumed to be R_e, and

$$F_3 = \int_o^1 \frac{\xi_1(1-\xi_1^{3/2})}{1 + P_2(1-\xi_1^{3/2})}\,d\xi_1$$

$$\cong \frac{0.21429 + 0.04061 P_2 - 0.01249 P_2^2 + 0.00351 P_2^3}{1 + 0.78948 P_2} \quad (A.38)$$

The factor $\rho_j u_j r_j^2 \frac{T_j R_j}{T_e \bar{R}}$ in Eq. (A.37) can be eliminated by using Eq. (A.9). Hence,

$$J = \frac{M}{u_j} \frac{P_1 F_1 - \mu P_2 F_3}{\mu P_1 F_1 + P_1^2 F_2} \tag{A.39}$$

$$\frac{\partial m}{\partial x} = 2\pi \frac{\partial}{\partial x} \frac{M}{u_j} \left(\frac{P_1 F_1 - \mu P_2 F_3}{\mu P_1 F_1 + P_1^2 F_2} \right) \tag{A.40}$$

According to Ricou and Spalding (Ref. 23) and Hill (Ref. 24),

$$\frac{d_o}{m_j} \left(\frac{\rho_j}{\rho_e} \right)^{1/2} \frac{\partial m}{\partial x} = \text{constant} \quad \text{for} \quad \mu = 0 .$$

Therefore, Eq. (A.40) can be written as

$$\frac{d_o}{m_j} \left(\frac{\rho_j}{\rho_e} \right)^{1/2} \frac{\partial m}{\partial x} = \frac{d_o}{m_j} \frac{M}{u_j} \frac{1}{(\bar{\rho}_e)^{1/2}} 2\pi \frac{\partial}{\partial x} \frac{P_1 F_1 - \mu P_2 F_3}{\mu P_1 F_1 + P_1^2 F_2} .$$

But

$$\frac{M}{m_j u_j} = \frac{\frac{1}{2} r_o^2 \rho_j u_j (u_j - u_e)}{\pi r_o^2 \rho_j u_j u_j} = \frac{1}{2\pi} (1 - \mu) .$$

It follows that

$$\frac{d_o}{m_j} \left(\frac{\rho_j}{\rho_e} \right)^{1/2} \frac{\partial m}{\partial x} = (1-\mu) d_o \frac{1}{(\bar{\rho}_e)^{1/2}} \frac{\partial}{\partial x} \frac{P_1 F_1 - \mu P_2 F_3}{\mu P_1 F_1 + P_1^2 F_2}$$

$$= \frac{2(1-\mu)}{\sqrt{\bar{\rho}_e}} \frac{\partial}{\partial \bar{x}} \frac{P_1 F_1 - \mu P_2 F_3}{\mu P_1 F_1 + P_1^2 F_2} \tag{A.41}$$

$$= \frac{2(1-\mu)}{\sqrt{\bar{\rho}_e}} \left\{ \frac{P_1' F_1 + P_1 F_1' - \mu P_2' F_3 - \mu P_2 F_3'}{\mu P_1 F_1 + P_1^2 F_2} \right.$$

$$\left. - \frac{(P_1 F_1 - \mu P_2 F_3)(\mu P_1' F_1 + \mu P_1 F_1' + 2 P_1 P_1' F_2 + P_1^2 F_2')}{(\mu P_1 F_1 + P_1^2 F_2)^2} \right\} \frac{d\xi}{d\bar{x}} \tag{A.42}$$

where $' = \frac{d}{d\xi}$. In consistence with the turbulent jet model, the derivatives in Eq. (A.42) will be evaluated far downstream and then extrapolated to the near field. Hence,

$$P_1' = \frac{dP_1}{d\xi} \longrightarrow \frac{d}{d\xi} \left(\frac{1-\mu}{2\xi} \right) = -\frac{1-\mu}{2\xi^2} \longrightarrow -\frac{2P_1^2}{1-\mu} \tag{A.43}$$

$$P_2(\xi_R) = \left[\theta - 1 + \frac{1}{2}(1-\mu^2)(\gamma-1) M_j^2 \theta \right] H_o(\xi_R) -$$

$$- \frac{\gamma-1}{2} P_1(\xi) M_j^2 \theta \left[P_1(\xi) + 2\mu \right]$$

$$P_2'(\xi_R) = \left[\theta - 1 + \frac{1}{2}(1-\mu^2)(\gamma-1) M_j^2 \theta \right] H_o'(\xi_R) -$$

$$- \frac{\gamma-1}{2} P_1' M_j^2 \theta \left[P_1 + 2\mu \right] - \frac{\gamma-1}{2} P_1(\xi) M_j^2 \theta P_1'(\xi) \tag{A.44}$$

$$H_0'(\xi_{j_1}) \longrightarrow \frac{d}{d\xi_{j_1}}\left(\frac{1}{2\xi_{j_1}}\right)\frac{d\xi_{j_1}}{d\xi_j} = -\frac{1}{P_r}\frac{1}{2\xi_{j_1}^2} \longrightarrow -\frac{2H_0^2(\xi_{j_1})}{P_r} \qquad (A.45)$$

$$F_1' = -P_2'\int_0^1 \frac{\xi_1(1-\xi_1^{3/2})^3\, d\xi_1}{[1+P_2(1-\xi_1^{3/2})]^2}$$

$$\cong -P_2'\frac{0.08901 - 0.04005P_2 + 0.01792P_2^2 - 0.00646P_2^3}{1+1.05001P_2} \qquad (A.46)$$

$$F_2' = -P_2'\int_0^1 \frac{\xi_1(1-\xi_1^{3/2})^5\, d\xi_1}{[1+P_2(1-\xi_1^{3/2})]^2}$$

$$\cong -P_2'\frac{0.05270 - 0.02886P_2 + 0.01478P_2^2 - 0.00589P_2^3}{1+1.08869P_2} \qquad (A.47)$$

$$F_3' = -P_2'\int_0^1 \frac{\xi_1(1-\xi_1^{3/2})^2\, d\xi_1}{[1+P_2(1-\xi_1^{3/2})]^2}$$

$$\cong -P_2'\frac{0.12857 - 0.04653P_2 + 0.01820P_2^2 - 0.00599P_2^3}{1+1.02272P_2} \qquad (A.48)$$

One special application of Eq. (A.42) is the isothermal mixing so that $P_2 = 0$. Eq. (A.42) is reduced to

$$\frac{d_0}{m_j}\left(\frac{\rho_j}{\bar{\rho}_e}\right)^{1/2}\frac{\partial m}{\partial x} = \frac{2(1-\mu)}{\sqrt{\bar{\rho}_e}}\left\{\frac{P_1'F_1}{\mu P_1F_1+P_1^2F_2} - \frac{(P_1F_1)(\mu P_1'F_1+2P_1P_1'F_2)}{(\mu P_1F_1+P_1^2F_2)^2}\right\}\frac{d\xi}{d\bar{x}}$$

$$= \frac{2(1-\mu)}{\sqrt{\bar{\rho}_e}}\frac{-P_1'F_1F_2P_1^2}{(\mu P_1F_1+P_1^2F_2)^2}\frac{d\xi}{d\bar{x}}$$

$$= \frac{2(1-\mu)}{\sqrt{\bar{\rho}_e}}\frac{-F_1F_2\left(-\frac{2P_1^2}{1-\mu}\right)}{(\mu F_1+P_1F_2)^2}\cdot 2k_1(\bar{\rho}_e)^{1/2}\sqrt{\frac{1-\mu}{\mu}}\sqrt{P_1}\left[\ln\frac{1+\frac{2\mu}{P_1}}{1+\frac{\mu}{P_1}}\right]^{1/2}$$

$$= 8k_1F_1F_2\frac{P_1^2}{(\mu F_1+P_1F_2)^2}\sqrt{\frac{1-\mu}{\mu}}\sqrt{P_1}\left[\ln\frac{1+\frac{2\mu}{P_1}}{1+\frac{\mu}{P_1}}\right]^{1/2} \qquad (A.49)$$

This expression is independent of density ratio is k_1 is also independent of it. As $\xi_j \to 0$, the entrainment at the end of the potential core can be obtained:

$$\frac{d_0}{m_j}\left(\frac{\rho_j}{\bar{\rho}_e}\right)^{1/2}\frac{\partial m}{\partial x} = \frac{8k_1F_1F_2(1-\mu)^3}{[\mu F_1+(1-\mu)F_2]^2\sqrt{\mu}}\left\{\ln\frac{1+\frac{2\mu}{1-\mu}}{1+\frac{\mu}{1-\mu}}\right\}^{1/2} \qquad (A.50)$$

A special case is $\mu = 0$. It can be shown from Eq. (A.50) that the entrainment function is a constant and is equal to

$$\frac{d_o}{m_j}\left(\frac{\rho_j}{\rho_e}\right)^{1/2}\frac{\partial m}{\partial x} = 8k_1\frac{F_1}{F_2} = \frac{8k_1 \times 0.12857}{0.06676} \qquad (A.51)$$

which depends on the value of k_1. Therefore, to complete the theory, it is necessary to choose k_1 such that best correlation with experimental data can be obtained.

It is of interest to note that different values of k_1 have been used by different authors in the past (Refs. 25 and 26). In Prandtl's model for uniform density mixing, it is assumed that

$$\varepsilon = k_1 b_{1/2}(u_c - u_e) \qquad (A.52)$$

and k_1 has been taken as 0.022. In Ferri's model,

$$\rho\varepsilon = k_1 b_{1/2}(\rho_c u_c - \rho_e u_e) \qquad (A.53)$$

and k_1 was chosen as 0.025. In correlation with experimental data of free jets (with quiescent surrounding), Kleinstein found that $k_1 = 0.0185$. Recently, Witze (Ref. 27) re-correlated free-jet data and found that

$$k_1 = 0.02(1 - 0.16 M_j)\left(\frac{\rho_e}{\rho_j}\right)^{-0.22} \qquad (A.54)$$

Unfortunately, if Eq. (A.54) is used in Eq. (A.51), it would result in the entrainment function depending on the density ratio, contrary to the experimental conclusion by Ricou and Spalding (Ref. 23). A more complicated model was proposed by Boyle and Viets (Ref. 25):

$$\rho\varepsilon = K b_{1/2}(\rho_c u_c - \rho_e u_e)\left(\frac{\rho_e}{\rho_j}\right)^{1/2}\left[\frac{\rho_j u_j - \rho_e u_e}{\rho_c u_c - \rho_e u_e}\right]^{\lambda}$$

$$\lambda = \frac{\rho_e u_e}{\rho_j u_j} \qquad (A.55)$$

where $K = 0.022$ in the main region of the jet. According to this model, the effective mixing length in the far field is greater for jets in a coflowing stream than for free jets because of the last factor in Eq. (A.55). Comparing (A.53) with Eq. (A.55), it is reasonable to assume that k_1 in Eq. (A.53) increases with the velocity ratio $u_e/u_j\ (=\mu)$.

To keep the method as simple as possible, it is assumed in the present method that $k_1 = 0.0185$ for $\mu = 0$, as used by Kleinstein. At $\mu = 0.5$, different values of k_1 have been tried and the results for the centerline velocity decay compared with experimental data. Reasonably good agreement was obtained if $k_1 = 0.024$. This is shown in Fig. A.2. For other values of μ, a linear interpolation or extrapolation gives

$$k_1 = 0.0185 + 0.011\mu \tag{A.56}$$

To show the accuracy of Eq. (A.56), comparison with experimental data and the computation of Boyle and Viets is presented in Figs. A.1 - A.9. The turbulent Prandtl number is assumed constant and taken to be 0.72. It is seen that the results of the present method are reasonably good, except Fig. (A.5a) where the experimental data show different trend from those of Fig. A.2, even though the density ratio is only slightly different.

With Eq. (A.56), Eq. (A.51) shows that for $\mu = 0$, $\frac{d_o}{m_j}\left(\frac{\rho_j}{\rho_e}\right)^{1/2}\frac{\partial m}{\partial x} = 0.285$. This is to be compared with the experimental value of 0.32 by Ricou and Spalding (Ref. 23) and Hill (Ref. 24). This difference may be attributed to the assumed form of η_u, as has been discussed by Ricou and Spalding. To see how the assumed velocity profiles would affect the entrainment, let

$$\frac{u - u_e}{u_c - u_e} = \frac{1}{2}\left(1 + \cos \pi \xi_1\right) \tag{A.57}$$

Eq. (A.57) was used by Squire and Trouncer (Ref. 6). If Eq. (A.57) was used, Eq. (A.51) would become, for $\mu = 0$, $\theta = 1$, $\bar{\rho}_e = 1$,

$$\frac{d_o}{m_j}\left(\frac{\rho_j}{\rho_e}\right)^{1/2}\frac{\partial m}{\partial x} = \frac{8\pi_1 \pi\, 0.14868}{0.08618} \tag{A.58}$$

The ratio F_1/F_2 would be 1.725, instead of 1.926 in Eq. (A.51). This would further decrease the value of the entrainment function. Since F_1 is proportional to $(u - u_e)$, while F_2 is proportional to $(u - u_e)^2$,

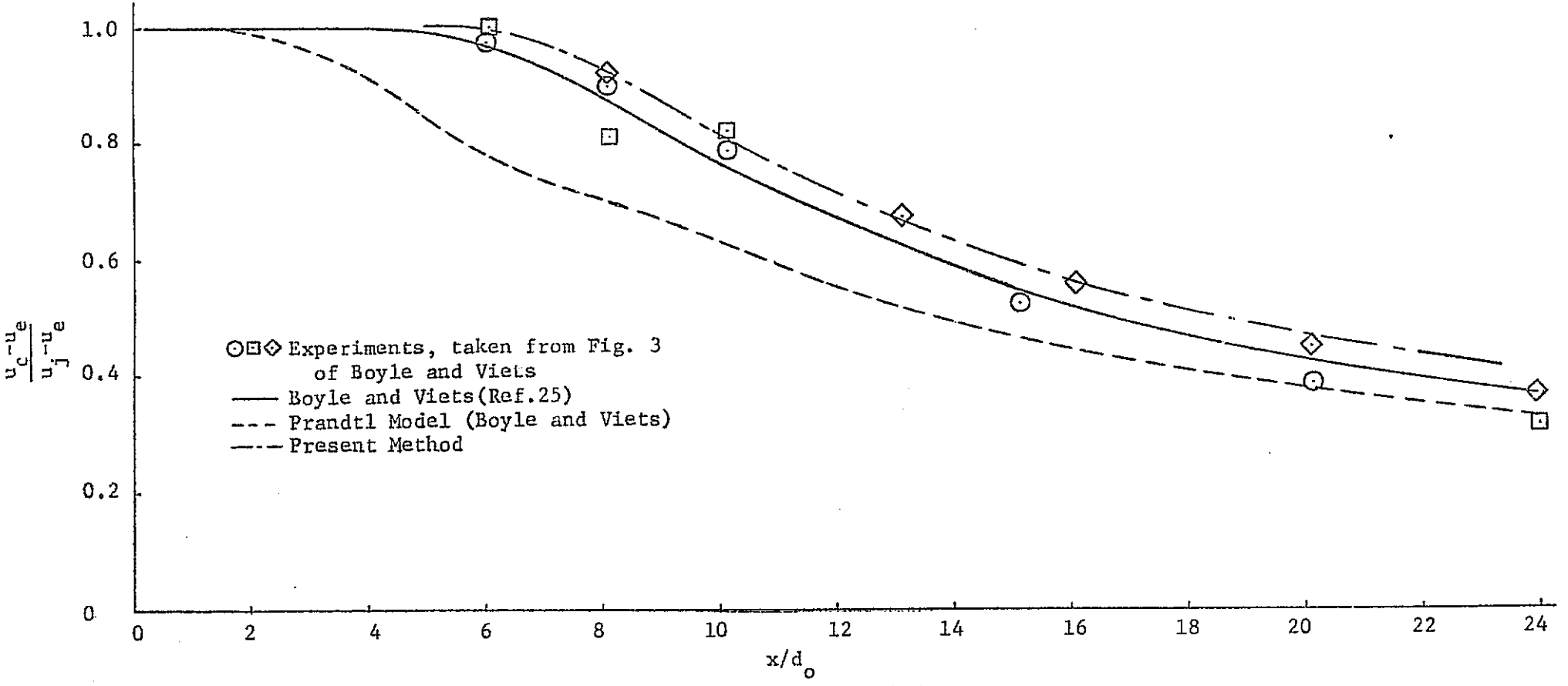

Figure A.1 Theory and Experiments for Turbulent Jet Mixing.
$\rho_e/\rho_j=1$, $T_j/T_e=1$, $\mu=0.25$ and $M_j=0$

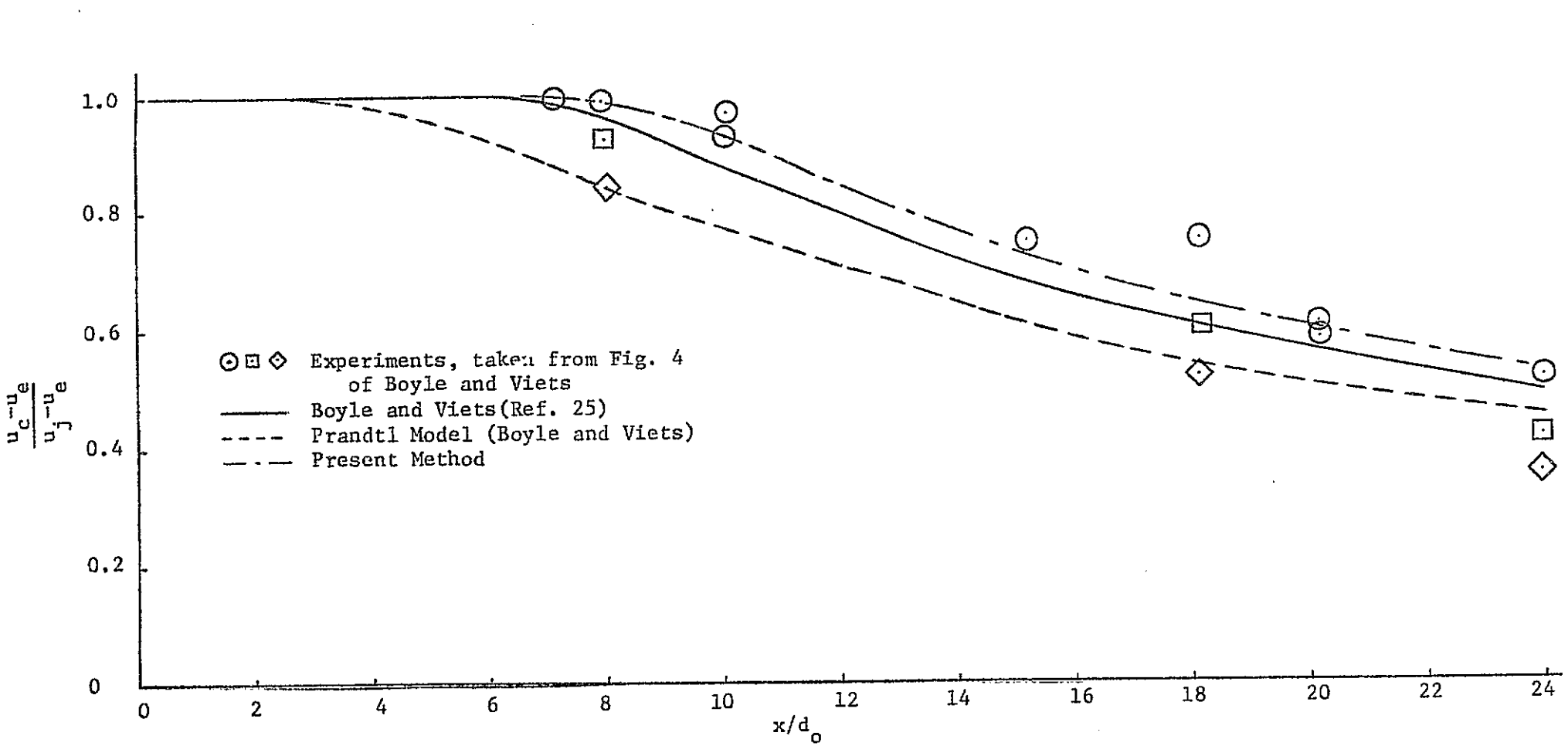

Figure A.2 Theory and Experiments for Turbulent Jet Mixing.
$\rho_e/\rho_j=1$, $T_j/T_e=1$, $\mu=0.5$ and $M_j=0$

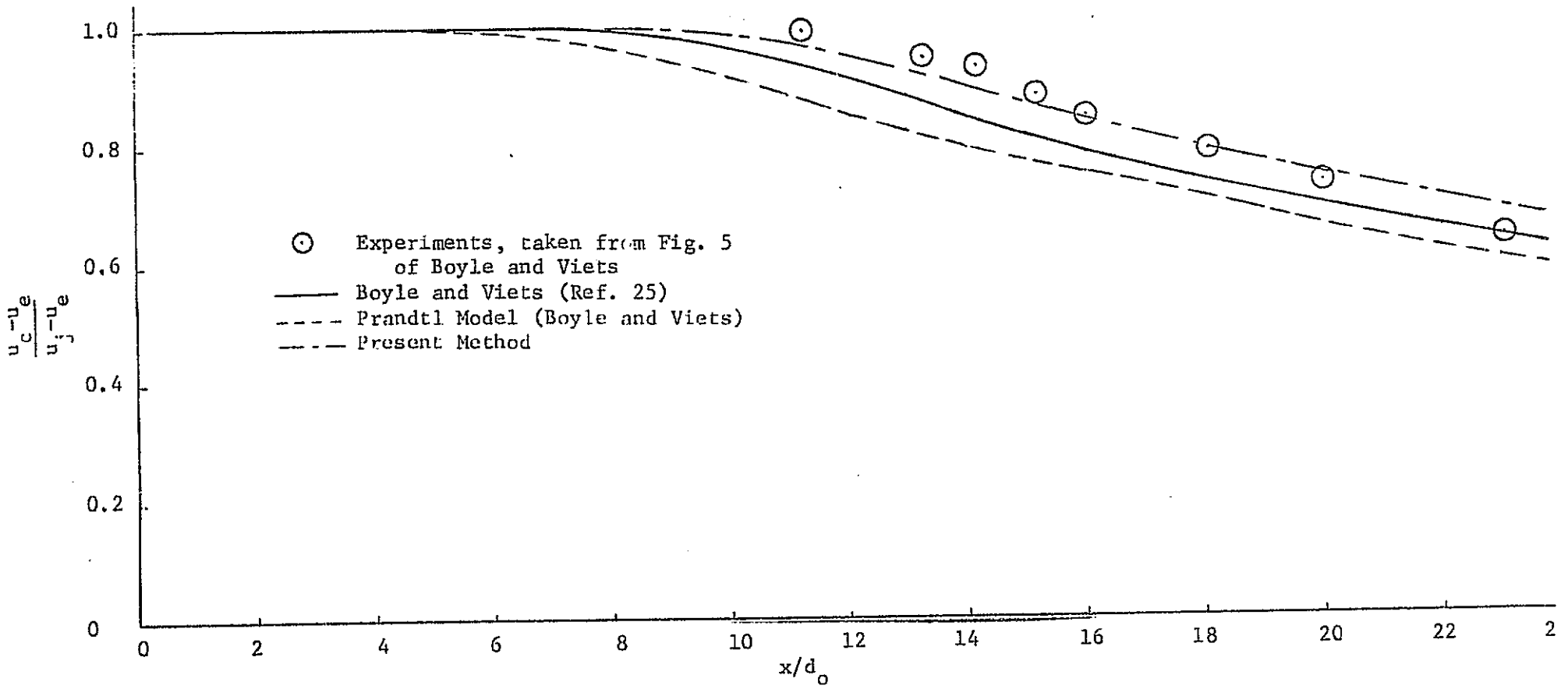

Figure A.3 Theory and Experiments for Turbulent Jet Mixing.
$\rho_e/\rho_j=1$, $T_j/T_e=1$, $\mu=0.67$ and $M_j=0$

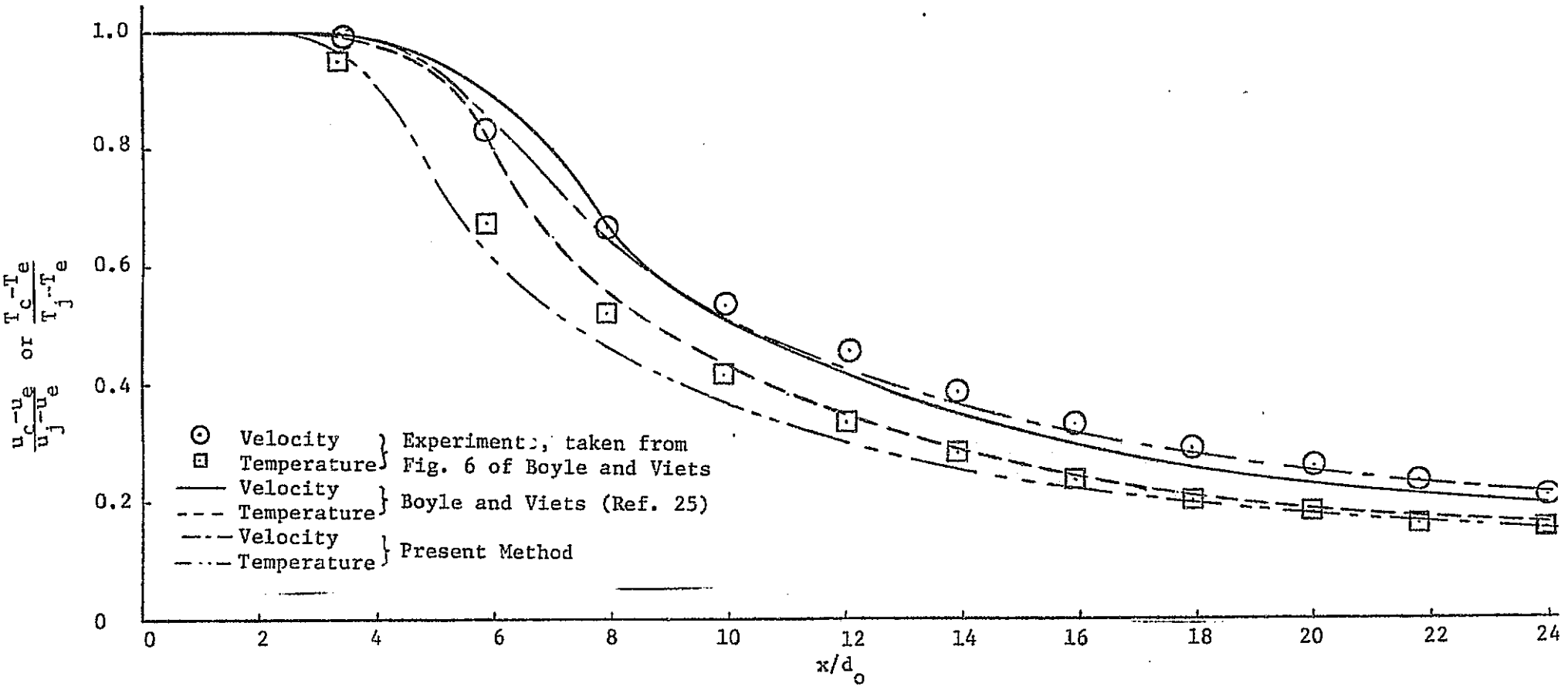

Figure A.4 Theory and Experiments for Turbulent Jet Mixing.
$\rho_e/\rho_j=2$, $T_j/T_e=2$, $\mu=0$ and $M_j=0.07$

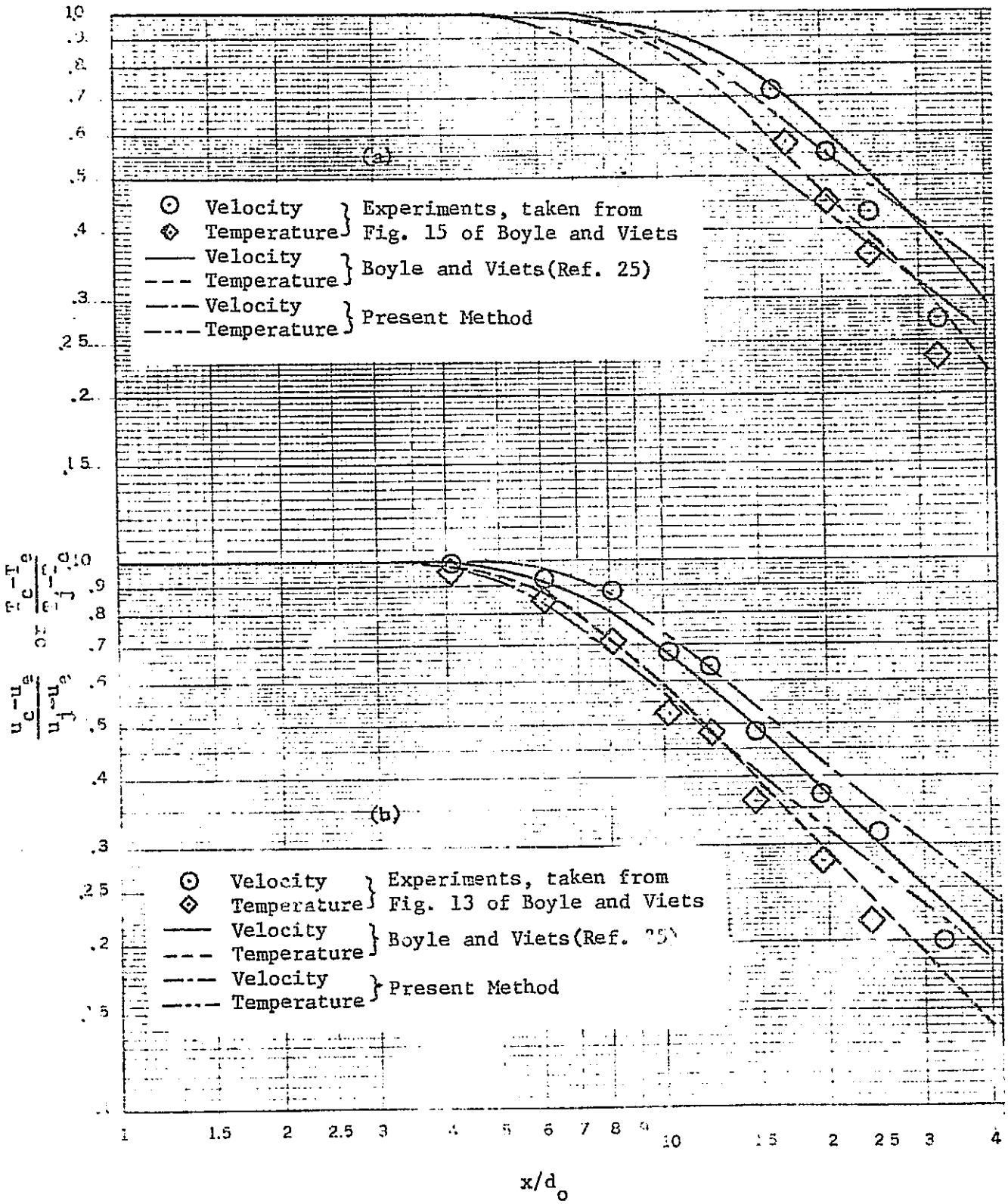

Figure A.5 Theory and Experiments for Turbulent Jet Mixing.
(a) $\rho_e/\rho_j=1.19$, $T_j/T_e=1.19$, $\mu=0.5$ and $M_j=0.1$
(b) $\rho_e/\rho_j=1.296$, $T_j/T_e=1.296$, $\mu=0.25$ and $M_j=0.1$

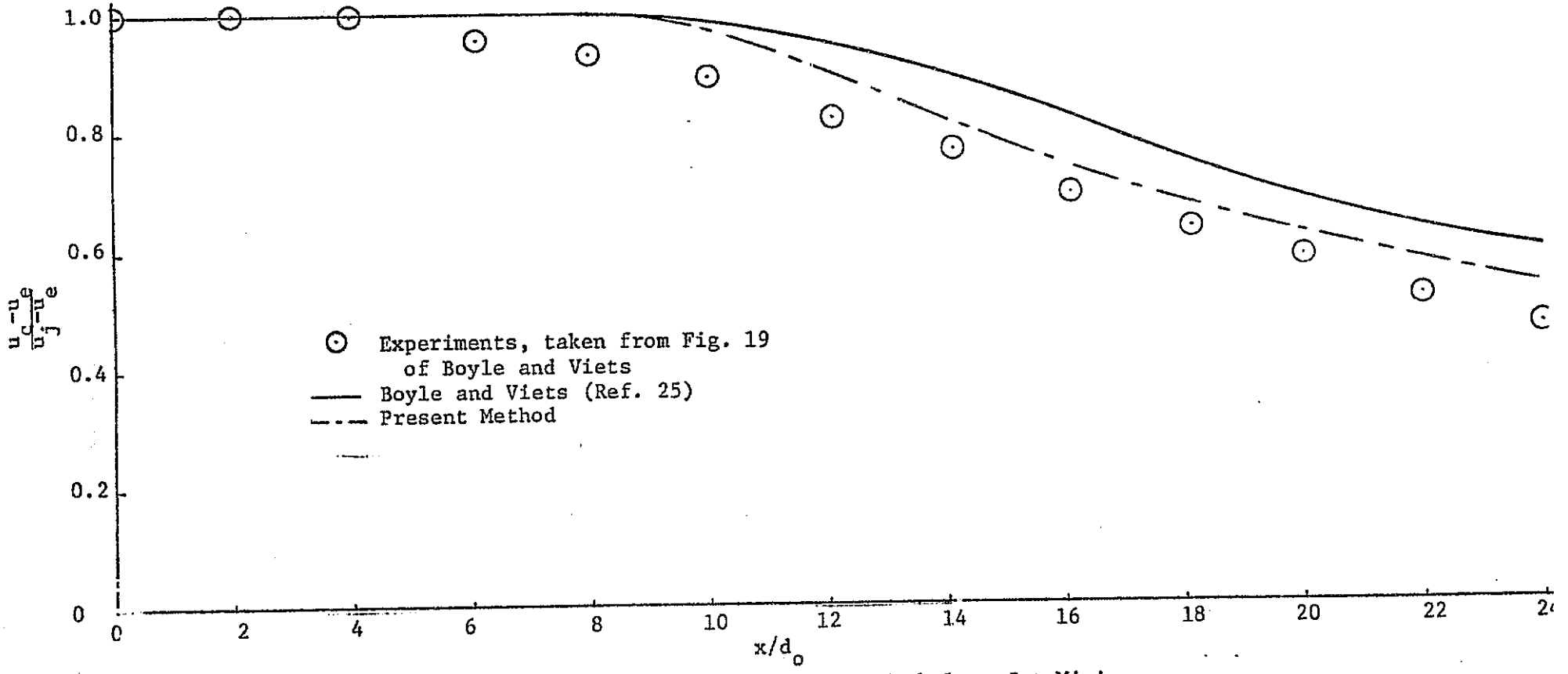

Figure A.6 Theory and Experiments for Turbulent Jet Mixing.
$\rho_e/\rho_j=0.51$, $T_j/T_e=1$, $\mu=0.253$ and $M_j=0.2$

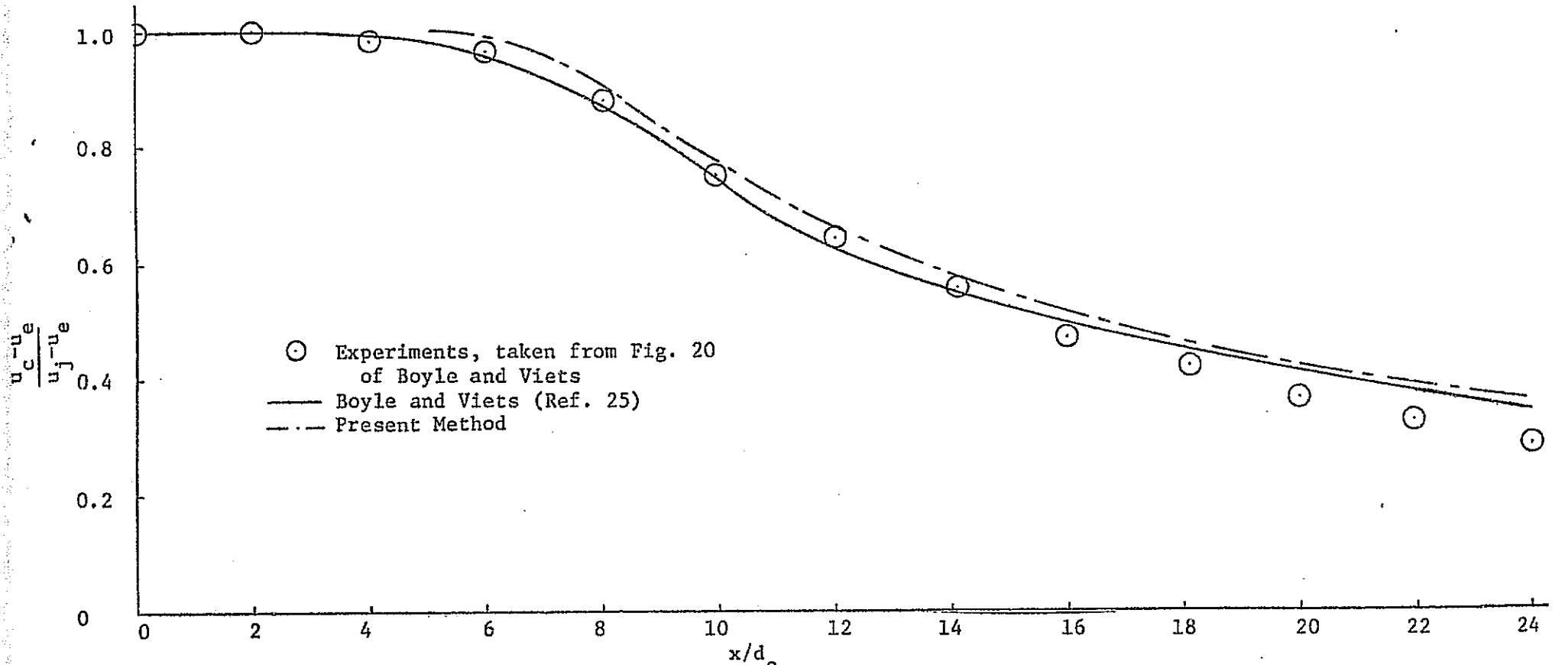

Figure A.7 Theory and Experiments for Turbulent Jet Mixing.
$\rho_e/\rho_j=1$, $T_j/T_e=1$, $\mu=0.131$ and $M_j=0.4$

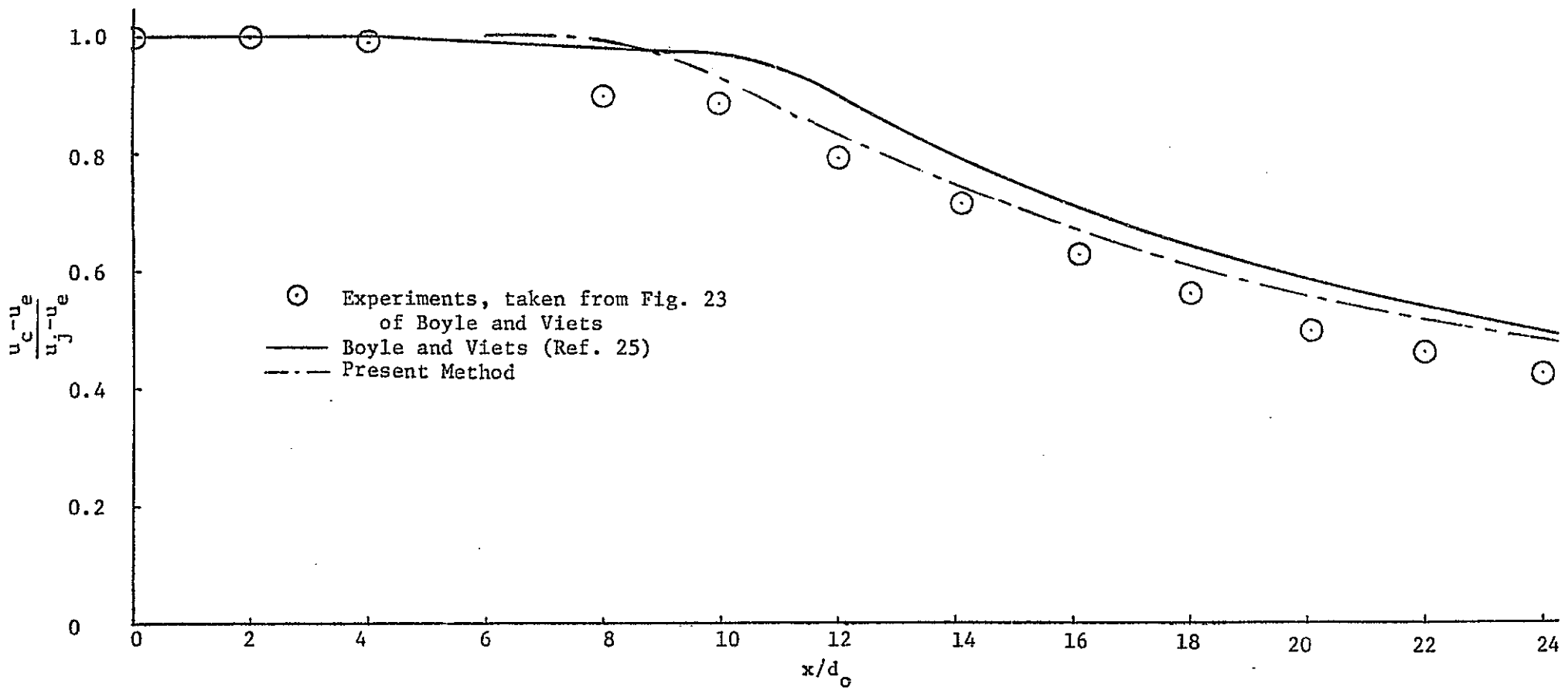

Figure A.8 Theory and Experiments for Turbulent Jet Mixing.
ρ_e/ρ_j=0.67, T_j/T_e=1, μ=0.261 and M_j=0.2

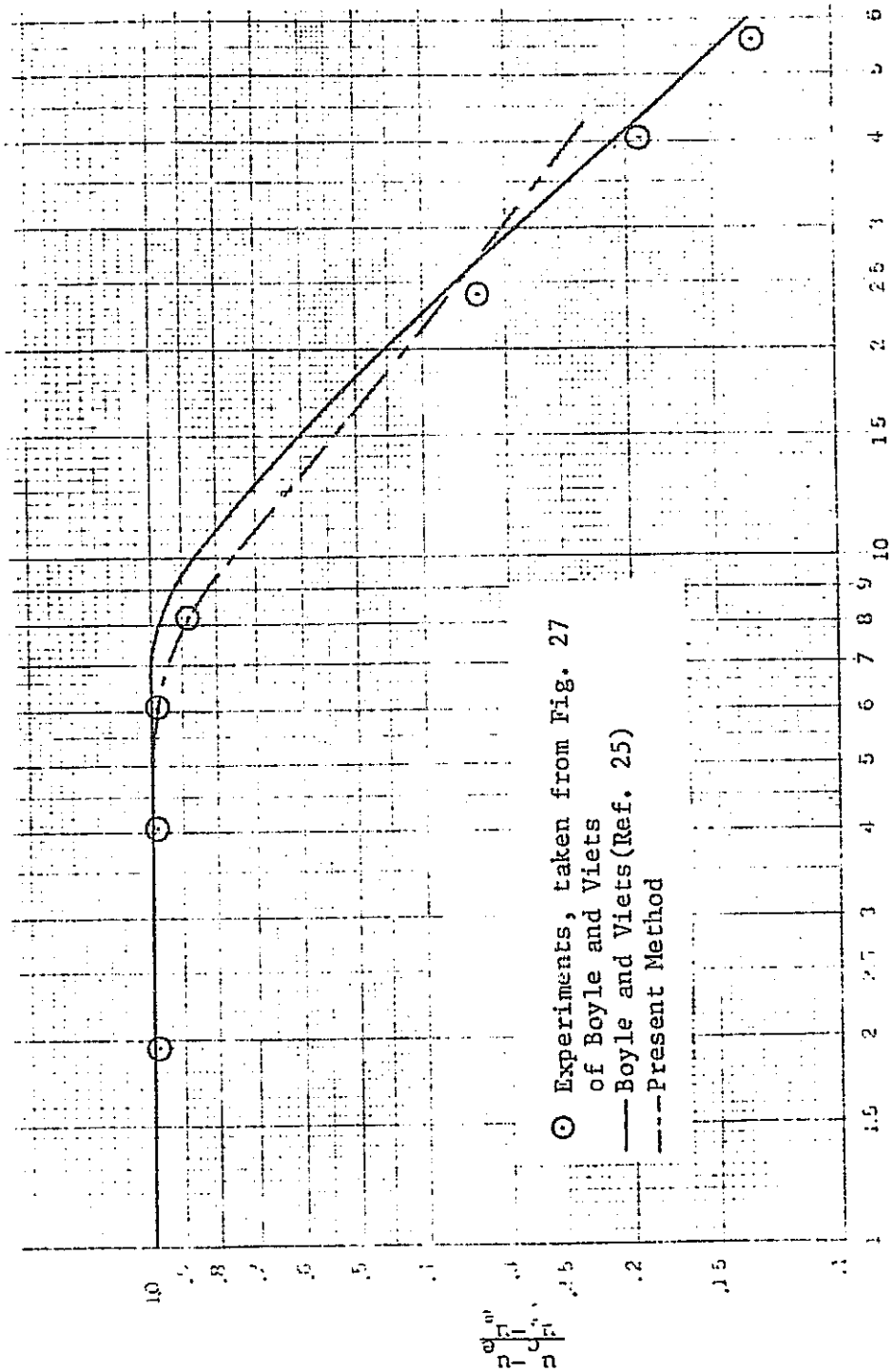

Figure A.9 Theory and Experiments for Turbulent Jet Mixing.
ρ_e/ρ_j=1.09, T_j/T_e=1., μ=0.2 and M_j=0.2

it seems reasonable to assume that F_1 should be replaced by SF_1 and F_2 by S^2F_2, where S may be called the shape factor of the velocity profile. If this assumption is made in Eq. (A.51), then

$$\frac{d_o}{m_j}\left(\frac{\rho_j}{\rho_e}\right)^{1/2}\frac{\partial m}{\partial x} = \frac{8k_1 \times 0.1\text{=}857}{0.06676\,S}$$

With $k_1 = 0.0185$, this value is to be equated to 0.32 to give $S = 0.8907$. The reasonableness of the shape factor can be demonstrated by using Squire and Trouncer's velocity profile. If Eq. (A.57) is used, $F_1 = 0.14868$. This can be reduced to the present value of 0.12857 by using a shape factor of 0.865. Then $F_2 = 0.08618$ by Eq. (A.57) will be reduced to $(0.865)^2 \times 0.08618 = 0.0645$ which differs only 3% from the correct value of 0.06676. It may be summarized that for the present application, in all expressions developed so far,

$$F_1 \text{ be replaced by } 0.8907F_1, \text{ and } F_2 \text{ by } (0.8907)^2F_2. \qquad \text{(A.59)}$$

F_3 remains unchanged; i.e., the temperature profile will be assumed to be correct.

Entrainment in the initial region

The entrainment function will be assumed to vary linearly in the initial region. At the end of the potential core region, the value of the entrainment function is obtained by the above theory. At the exit, it will be obtained by Abramovich's theory. Since the latter does not account for compressibility effects, it will be applied in the following manner. For a free jet with uniform density and isothermal mixing the entrainment at the jet exit can be obtained by Abramovich theory. Under other conditions, the entrainment at the exit will be changed proportionally in the same way as that at the end of the potential core being changed relative to the free jet value.

According to Abramovich's theory, the inflow velocity at the exit for uniform density and isothermal mixing in a free jet is given by [p. 306 of Ref. 21]

$$\frac{v_{je}}{u_j} = 0.27\,(B-A) \tag{A.60}$$

where A = 0.316 and B = 0.450 (p. 282 of Ref. 21). Hence,

$$\frac{\partial m}{\partial x} = 2\pi r_o \rho v_{je}$$

$$\frac{d_o}{m_j}\left(\frac{\rho_j}{\rho_e}\right)^{1/2}\frac{\partial m}{\partial x} = \frac{(2r_o)\,2\pi r_o \rho}{\rho u_j \pi r_o^2} \times 0.27\,(0.45-0.316) \cong 0.145 \tag{A.61}$$

A.3 Comparison with Known Results

It should be noted that the present method is applicable to non-uniform density and/or non-isothermal mixing with compressibility effects. The compressibility effects are accounted for through Kleinstein's theory.

The model of Squire and Trouncer in uniform density and isothermal mixing is compared with the present one in Fig. A.10. For a free jet, the Squire and Trouncer's results are computed by using the data shown in Table 1 of Ref. 6; while the other two curves are constructed with the information given in Tables 2 and 3 of the same Reference. Note that to convert Squire and Trouncer's results to the present notation, the following relation is needed:

$$\frac{\partial m}{\partial x} = 2\pi \rho_e \frac{\partial \psi}{\partial x} \tag{A.62}$$

Since $m_j = \pi r_o^2 \rho_j u_j$, it follows that for $\rho_e = \rho_j$,

$$\frac{d_o}{m_j}\left(\frac{\rho_j}{\rho_e}\right)^{1/2}\frac{\partial m}{\partial x} = \frac{d_o}{m_j}\frac{\partial m}{\partial x} = 4\left(\frac{1}{u_j r_o}\frac{\partial \psi}{\partial x}\right) \tag{A.63}$$

It is seen from Fig. A.10 that Squire and Trouncer's model gives higher entrainment in the initial region of the jet and lower values in the fully developed portion. The difference with the present method becomes small as M is increased.

To find the effects of entrainment on the aerodynamic characteristics,

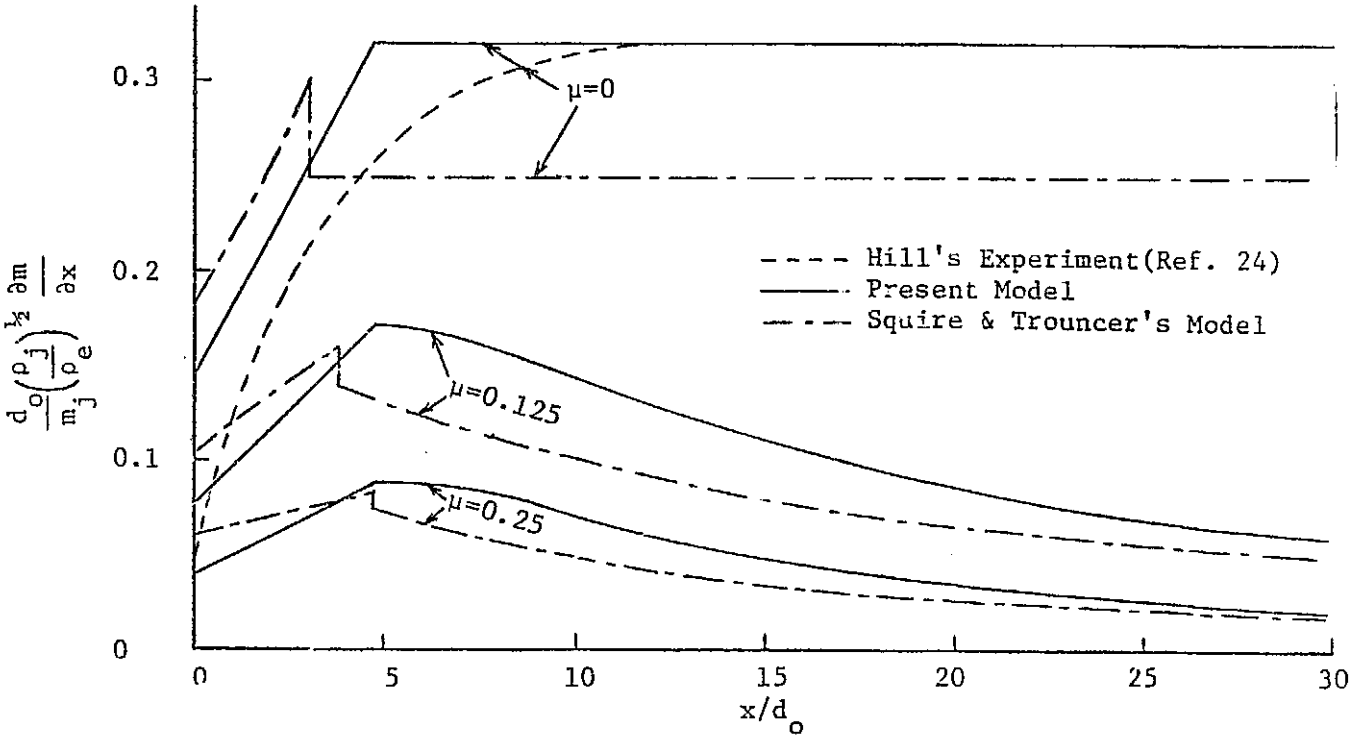

Figure A.10 Comparison of Entrainment Models. $\rho_e/\rho_j=1$, $T_j/T_e=1$ and $M_j=0$

a line sink distribution is placed on the jet axis with strength equal to the entrained volume flow rate:

$$q_b = \frac{1}{\rho_j}\frac{\partial m}{\partial x} \tag{A.64}$$

Let

$$\frac{d_o}{m_j}\left(\frac{\rho_j}{\rho_e}\right)^{1/2}\frac{\partial m}{\partial x} = E(\bar{x}) \tag{A.65}$$

Then

$$q_b = \frac{1}{\rho_j}E(\bar{x})\frac{m_j}{d_o}(\bar{\rho}_e)^{1/2} = E(\bar{x})\frac{\pi r_o^2 \rho_j u_j}{2\rho_j r_o}(\bar{\rho}_e)^{1/2}$$

$$= \frac{\pi}{2}u_j r_o(\bar{\rho}_e)^{1/2}E(\bar{x}) \tag{A.66}$$

The corresponding induced velocity components due to the sink distribution can be computed as (Ref. 15)

$$\frac{\partial\phi}{\partial\bar{r}} = -\frac{\beta^2\bar{r}}{4\pi}\int_0^\infty \frac{q_b(\bar{\xi})\,d\bar{\xi}}{\left[(\bar{x}-\bar{\xi})^2+\beta^2\bar{r}^2\right]^{3/2}} \tag{A.67}$$

$$\frac{\partial\phi}{\partial\bar{x}} = -\frac{1}{4\pi}\int_0^\infty \frac{q_b(\bar{\xi})(\bar{x}-\bar{\xi})\,d\bar{\xi}}{\left[(\bar{x}-\bar{\xi})^2+\beta^2\bar{r}^2\right]^{3/2}} \tag{A.68}$$

In application, the jet axis is divided into segments within which $q_b(\bar{\xi})$ or $E(\bar{\xi})$ is assumed to vary linearly. Let

$$E(\bar{\xi}) = a_i + b_i\bar{\xi} \tag{A.69}$$

in the ith interval. Then

$$\frac{\partial\phi}{\partial\bar{r}} = -\frac{1}{4\pi}\beta^2\bar{r}\,\frac{\pi}{2}u_j r_o(\bar{\rho}_e)^{1/2}\sum_i\int_{\bar{x}_i}^{\bar{x}_{i+1}}\frac{(a_i+b_i\bar{\xi})\,d\bar{\xi}}{\left[(\bar{x}-\bar{\xi})^2+\beta^2\bar{r}^2\right]^{3/2}}$$

or,

$$\frac{1}{u_j r_o}\frac{\partial\phi}{\partial\bar{r}} = -\frac{(\bar{\rho}_e)^{1/2}}{8}\beta^2\bar{r}\sum_i\int_{\bar{x}_i}^{\bar{x}_{i+1}}\frac{(a_i+b_i\bar{\xi})\,d\bar{\xi}}{\left[(\bar{x}-\bar{\xi})^2+\beta^2\bar{r}^2\right]^{3/2}} \tag{A.70}$$

Similarly,

$$\frac{1}{u_j r_o}\frac{\partial\phi}{\partial\bar{x}} = -\frac{(\bar{\rho}_e)^{1/2}}{8}\sum_i\int_{\bar{x}_i}^{\bar{x}_{i+1}}\frac{(a_i+b_i\bar{\xi})(\bar{x}-\bar{\xi})\,d\bar{\xi}}{\left[(\bar{x}-\bar{\xi})^2+\beta^2\bar{r}^2\right]^{3/2}} \tag{A.71}$$

The integrals in Eqs. (A.70) and (A.71) can be exactly integrated to give

$$\int_{\bar{x}_i}^{\bar{x}_{i+1}}\frac{(a_i+b_i\bar{\xi})\,d\bar{\xi}}{\left[(\bar{x}-\bar{\xi})^2+\beta^2\bar{r}^2\right]^{3/2}} = -\frac{a_i+b_i\bar{x}}{\beta^2\bar{r}^2}G_{1i} - b_i G_{2i} \tag{A.72}$$

$$\int_{\bar{x}_i}^{\bar{x}_{i+1}} \frac{(a_i+b_i\bar{\xi})(\bar{x}-\bar{\xi})\,d\bar{\xi}}{[(\bar{x}-\bar{\xi})^2+\beta^2\bar{r}^2]^{3/2}} = (a_i+b_i\bar{x})\,G_{2i} - b_i\,G_{1i} +$$

$$+ b_i \ln \frac{\bar{x}-\bar{x}_{i+1}+\sqrt{(\bar{x}-\bar{x}_{i+1})^2+\beta^2\bar{r}^2}}{\bar{x}-\bar{x}_i+\sqrt{(\bar{x}-\bar{x}_i)^2+\beta^2\bar{r}^2}} \qquad \text{(A.73)}$$

$$G_{1i} = \frac{\bar{x}-\bar{x}_{i+1}}{\sqrt{(\bar{x}-\bar{x}_{i+1})^2+\beta^2\bar{r}^2}} - \frac{\bar{x}-\bar{x}_i}{\sqrt{(\bar{x}-\bar{x}_i)^2+\beta^2\bar{r}^2}} \qquad \text{(A.74)}$$

$$G_{2i} = \frac{1}{\sqrt{(\bar{x}-\bar{x}_{i+1})^2+\beta^2\bar{r}^2}} - \frac{1}{\sqrt{(\bar{x}-\bar{x}_i)^2+\beta^2\bar{r}^2}} \qquad \text{(A.75)}$$

The above formulation is now applied to find the pressure distribution due to entrainment on an infinite plane wall with a cold jet exhausting normally from it. The wall boundary condition can be satisfied by using an image sink distribution. The results of using this image system is to cancel the velocity component $\frac{\partial\phi}{\partial x}$ at x = 0 (i.e., on the wall) and the velocity $\frac{\partial\phi}{\partial r}$ on the wall is doubled over the value when the wall is non-existing. Using the present model, the induced velocity on the wall is given by

$$\frac{1}{u_j r_o}\frac{\partial\phi}{\partial\bar{r}} = -2x\frac{1}{8}\left\{-\frac{(a+b\bar{x})}{\bar{r}}G_1 - \beta^2 b\bar{r}\,G_2 + \frac{0.32}{\bar{r}}\left[1+\frac{\bar{x}-\bar{x}_c}{\sqrt{(\bar{x}-\bar{x}_c)^2+\beta^2\bar{r}^2}}\right]\right\}_{\bar{x}=0} \qquad \text{(A.76)}$$

where

$$a = 0.145 \quad , \quad b = 0.0185 \quad , \quad \bar{x}_c = 9.46$$

$$G_1 = \frac{\bar{x}-\bar{x}_c}{\sqrt{(\bar{x}-\bar{x}_c)^2+\beta^2\bar{r}^2}} - \frac{\bar{x}}{\sqrt{\bar{x}^2+\beta^2\bar{r}^2}} \quad , \bar{x}=0 \qquad \text{(A.77a)}$$

$$G_2 = \frac{1}{\sqrt{(\bar{x}-\bar{x}_c)^2+\beta^2\bar{r}^2}} - \frac{1}{\sqrt{\bar{x}^2+\beta^2\bar{r}^2}} \quad , \bar{x}=0 \qquad \text{(A.77b)}$$

For the Squire and Trouncer's model, the initial region is divided into 4 segments in accordance with the results shown on Table 1 of Ref. 6. The entrainment data are then computed by the method indicated there. The results are as shown below:

$$
\begin{aligned}
E(\bar{x}) &= 0.1823 + 0.01812\,\bar{x}\,, && 0 \le \bar{x} \le 1.49 \\
&= 0.13254 + 0.01796\,\bar{x}\,, && 1.49 \le \bar{x} \le 2.99 \\
&= 0.17949 + 0.01898\,\bar{x}\,, && 2.99 \le \bar{x} \le 4.48 \\
&= 0.15933 + 0.02348\,\bar{x}\,, && 4.48 \le \bar{x} \le 6.09 \\
&= 0.249\,, && \bar{x} > 6.09
\end{aligned}
\tag{A.78}
$$

$$
\frac{1}{u_j r_o}\frac{\partial \phi}{\partial \bar{r}} = -2\times\frac{1}{8}\left\{-\sum_{i=1}^{4}\left[\frac{a_i + b_i\bar{x}}{\bar{r}}\,G_{1i} + \beta^2 b_i \bar{r}\,G_{2i}\right] + \frac{0.249}{\bar{r}}\left[1 + \frac{\bar{x}-\bar{x}_c}{\sqrt{(\bar{x}-\bar{x}_c)^2+\beta^2\bar{r}^2}}\right]\right\}
\tag{A.79}
$$

$$\bar{x} = 0\,,\quad \bar{x}_c = 6.09$$

The pressure coefficient expressed in terms of jet dynamic pressure is given by

$$C_p = -\left(\frac{1}{u_j r_o}\frac{\partial \phi}{\partial \bar{r}}\right)^2 \tag{A.80}$$

The results are compared in Fig. A.11. The experiment was done by Gentry and Margason (Ref. 28) and Wygnanski's analytical results are given in Ref. 29. Both curves were taken directly from Fig. 1 of Ref. (30). It is seen that higher entrainment in the initial region in Squire and Trouncer's model yields slightly higher C_p than the experimental results and the present method. On the other hand, the present results are generally lower than the experimental values away from the jet boundary. It should be noted that small values of C_p are being compared which are very sensitive to the change of entrainment values near the jet exit.

Away from the wall, the inflow velocity can be computed as follows. Using the image sink distribution, it is obtained that

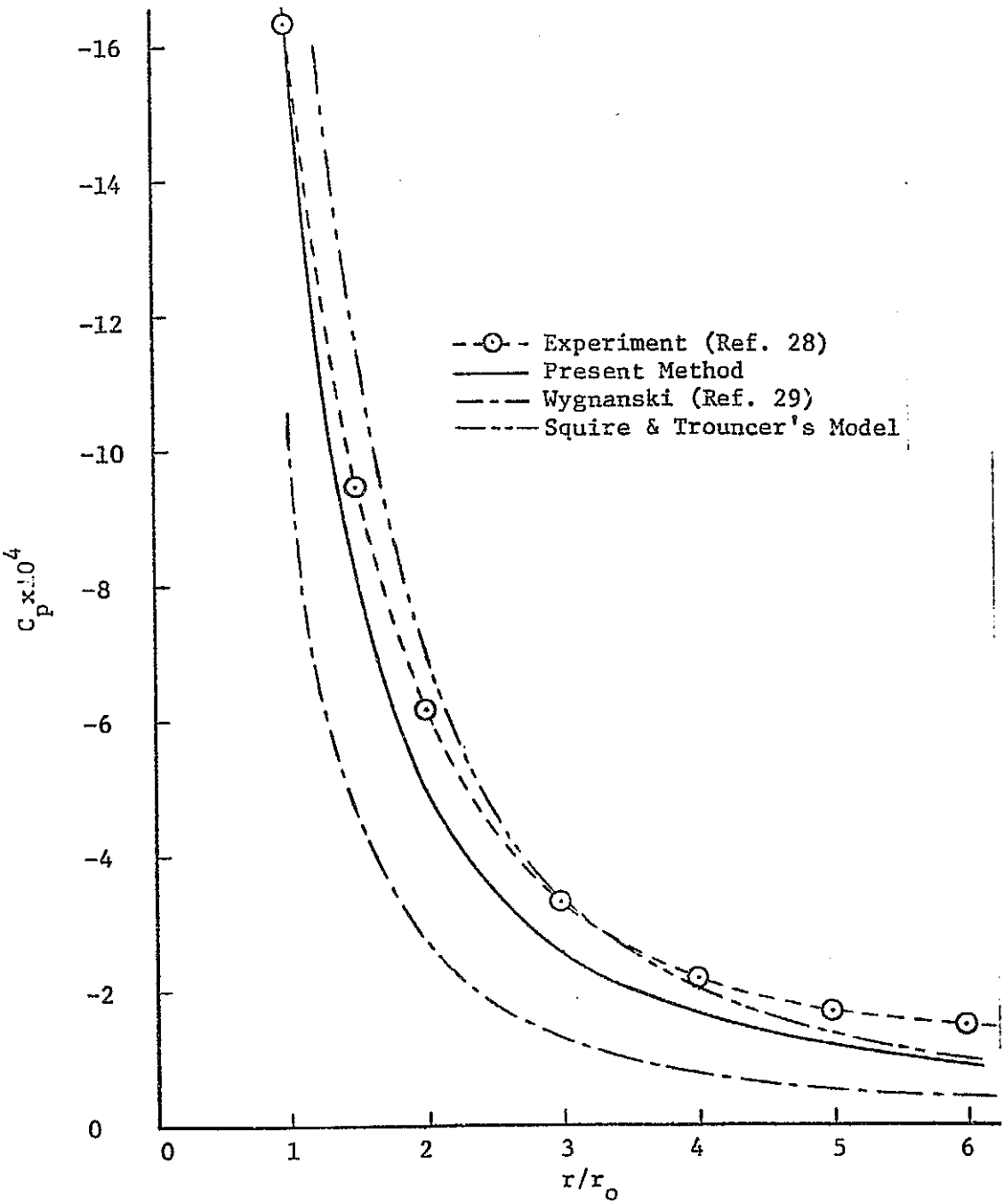

Figure A.11 Pressure Coefficient Induced by a Jet on a Large Plane Wall

$$\frac{\partial \phi}{\partial \bar{r}} = -\frac{\beta^2 \bar{r}}{4\pi}\left\{\int_{-\infty}^{0} \frac{g_0(\bar{\xi})\,d\bar{\xi}}{[(\bar{x}-\bar{\xi})^2+\beta^2\bar{r}^2]^{3/2}} + \int_{0}^{\infty} \frac{g_0(\bar{\xi})\,d\bar{\xi}}{[(\bar{x}-\bar{\xi})^2+\beta^2\bar{r}^2]^{3/2}}\right\}$$

$$= -\frac{\beta^2 \bar{r}}{4\pi}\int_0^{c'}\left\{\frac{1}{[(\bar{x}+\bar{\xi})^2+\beta^2\bar{r}^2]^{3/2}} + \frac{1}{[(\bar{x}-\bar{\xi})^2+\beta^2\bar{r}^2]^{3/2}}\right\} g_0(\bar{\xi})\,d\bar{\xi}$$

$$= -\frac{\beta^2 \bar{r}}{4\pi}\left\{-\frac{a+b\bar{x}}{\beta^2\bar{r}^2}G_1 - bG_2 + \frac{a-b\bar{x}}{\beta^2\bar{r}^2}G_1' - bG_2' + \right.$$

$$\left. + \frac{c'}{\beta^2\bar{r}^2}\left[1+\frac{\bar{x}-\bar{x}_c}{\sqrt{(\bar{x}-\bar{x}_c)^2+\beta^2\bar{r}^2}}\right] + \frac{c'}{\beta^2\bar{r}^2}\left[1-\frac{\bar{x}+\bar{x}_c}{\sqrt{(\bar{x}+\bar{x}_c)^2+\beta^2\bar{r}^2}}\right]\right\} \quad \text{(A.81)}$$

where

$$c' = \begin{cases} 0.32 & \text{, present model} \\ 0.249 & \text{, Squire and Trouncer's model .} \end{cases}$$

$$G_1' = \frac{\bar{x}+\bar{x}_c}{\sqrt{(\bar{x}+\bar{x}_c)^2+\beta^2\bar{r}^2}} - \frac{\bar{x}}{\sqrt{\bar{x}^2+\beta^2\bar{r}^2}} \quad \text{(A.82a)}$$

$$G_2' = \frac{1}{\sqrt{(\bar{x}+\bar{x}_c)^2+\beta^2\bar{r}^2}} - \frac{1}{\sqrt{\bar{x}^2+\beta^2\bar{r}^2}} \quad \text{(A.82b)}$$

The results on vertical planes normal to the jet axis and at $\bar{x}$ = 10 and $\bar{x}$ = 40, respectively, are shown in Figs. A.12 and A.13. As expected, the lower entrainment in the far field in the Squire and Trouncer's model results in lower inflow velocity.

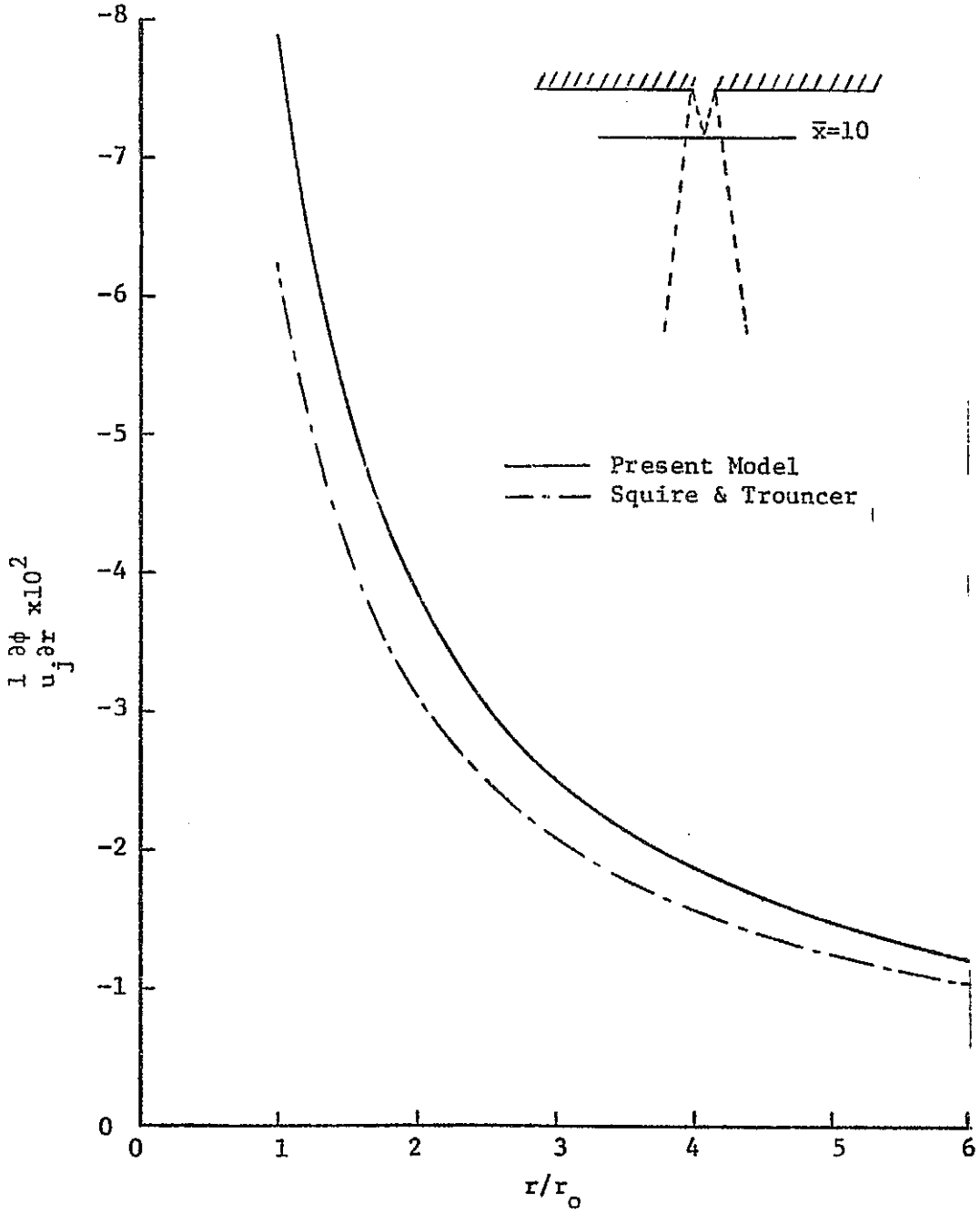

Figure A.12 Comparison of Computed Induced Inflow Velocity on a Plane at $\bar{x}$=10 due to a Jet Issuing from a Large Plane Wall by Two Entrainment Models

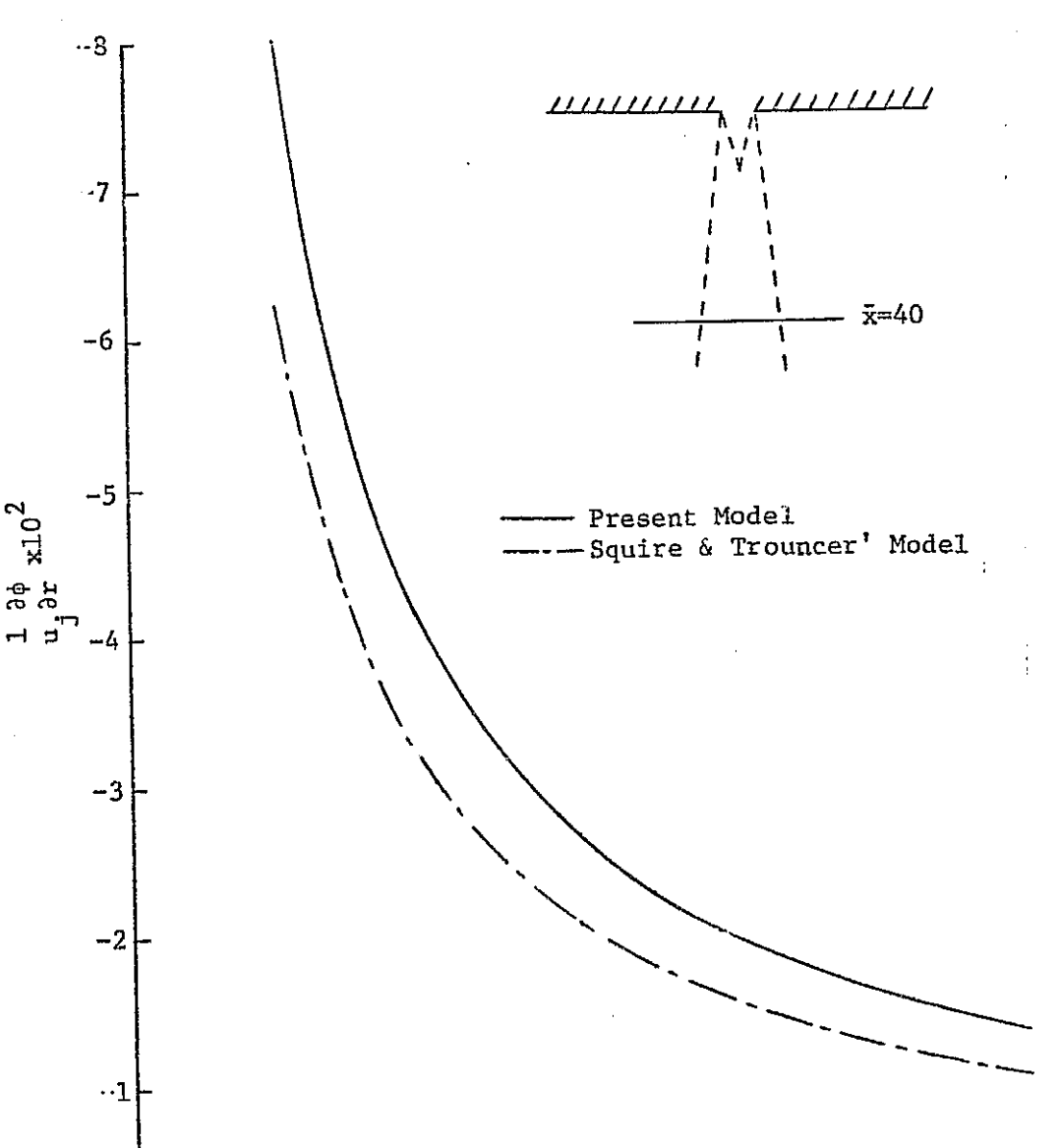

Figure A.13 Comparison of Computed Induced Inflow Velocity on a Plane at $\bar{x}$=40 due to a Jet Issuing from a Large Plane Wall by Two Entrainment Models.

Appendix B

Properties of an Equivalent Inviscid Jet

A turbulent jet has its properties varying not only in the axial direction but also in the radial direction. The perturbation in such a nonhomogeneous flow region would be governed by a partial differential equation with non-constant coefficients. To simplify the matter, an equivalent inviscid jet with uniform properties is used in the interaction computation in the present investigation. Such an equivalent jet is defined in accordance with the conservation of momentum, mass and heat content. Let the equivalent jet properties be denoted by $\tilde{\rho}_j$, $\tilde{u}_j$ and $\tilde{r}_j$. It follows from these conservation principles that

$$\int_0^{r_j} \frac{\rho u}{\rho_e u_e}\left(\frac{u}{u_e}-1\right)\frac{r}{r_0}\,d\left(\frac{r}{r_0}\right) = \frac{1}{2}\,\frac{\tilde{\rho}_j \tilde{u}_j}{\rho_e u_e}\left(\frac{\tilde{u}_j}{u_e}-1\right)\left(\frac{\tilde{r}_j}{r_0}\right)^2 \tag{B.1}$$

$$\int_0^{r_j}\left(\frac{\rho u}{\rho_e u_e}-1\right)\frac{r}{r_0}\,d\left(\frac{r}{r_0}\right) = \frac{1}{2}\left(\frac{\tilde{\rho}_j \tilde{u}_j}{\rho_e u_e}-1\right)\left(\frac{\tilde{r}_j}{r_0}\right)^2 \tag{B.2}$$

$$\begin{aligned}\int_0^{r_j} \frac{\rho u}{\rho_e u_e}\left(\frac{T}{T_e}-1\right)\frac{r}{r_0}\,d\left(\frac{r}{r_0}\right) &= \int_0^{r_j}\left(\frac{u}{u_e}-\frac{\rho u}{\rho_e u_e}\right)\frac{r}{r_0}\,d\left(\frac{r}{r_0}\right)\\ &= \frac{1}{2}\left(\frac{\tilde{u}_j}{u_e}-\frac{\tilde{\rho}_j \tilde{u}_j}{\rho_e u_e}\right)\left(\frac{\tilde{r}_j}{r_0}\right)^2\end{aligned} \tag{B.3}$$

The left-hand side of Eq. (B.1) can be written as

$$\begin{aligned}&\int_0^{r_j} \frac{\rho u}{\rho_e u_e}\left(\frac{u}{u_e}-1\right)\frac{r}{r_0}\,d\left(\frac{r}{r_0}\right) = \frac{\rho_j u_j}{\rho_e u_e}\left(\frac{r_j}{r_0}\right)^2 \frac{1}{\mu}\int_0^1 \frac{\rho u}{\rho_j u_j}\left(\frac{u}{u_j}-\mu\right)\xi_1\,d\xi_1\\ &= \frac{\rho_j u_j}{\rho_e u_e}\left(\frac{r_j}{r_0}\right)^2 \frac{1}{\mu}\left(P_1\mu F_1 + P_1^2 F_2\right)\frac{T_j R_j}{T_e \bar{R}}\end{aligned} \tag{B.4}$$

where Eq. (A.9) has been used . Hence, Eq. (B.1) becomes

$$\frac{1}{\mu^2}\left(\frac{r_j}{r_0}\right)^2\left(P_1\mu F_1 + P_1^2 F_2\right) = \frac{1}{2}\,\frac{\tilde{\rho}_j \tilde{u}_j}{\rho_e u_e}\left(\frac{\tilde{u}_j}{u_e}-1\right)\left(\frac{\tilde{r}_j}{r_0}\right)^2 \tag{B.5}$$

if $\rho_j T_j R_j / (\rho_e T_e \bar{R}) = 1$. Similarly, the left-hand side of Eq. (B.2) can be written as

$$\begin{aligned}&\left(\frac{r_j}{r_0}\right)^2 \int_0^1 \left(\frac{\rho u}{\rho_j u_j}\,\frac{1}{\bar{\rho}_e \mu}-1\right)\xi_1\,d\xi_1 = \left(\frac{r_j}{r_0}\right)^2 \frac{1}{\bar{\rho}_e \mu}\int_0^1 (\bar{\rho}\,\bar{u}-\bar{\rho}_e\mu)\xi_1\,d\xi_1\\ &= \left(\frac{r_j}{r_0}\right)^2 \frac{\rho_j}{\rho_e \mu}\,\frac{T_j R_j}{T_e \bar{R}}\left(P_1 F_1 - \mu P_2 F_3\right)\end{aligned} \tag{B.6}$$

where Eq. (A.37) has been used. It follows that Eq. (B.2) becomes

$$\frac{1}{\mu}\left(\frac{r_j}{r_o}\right)^2\left(P_1F_1 - \mu P_2 F_3\right) = \frac{1}{2}\left(\frac{\tilde{\rho}_j \tilde{u}_j}{\rho_e u_e} - 1\right)\left(\frac{\tilde{r}_j}{r_o}\right)^2 \qquad (B.7)$$

To integrate Eq. (B.3), note that

$$\int_0^{r_j}\left(\frac{u}{u_e} - \frac{\rho u}{\rho_e u_e}\right)\frac{r}{r_o}\,d\left(\frac{r}{r_o}\right) = \left(\frac{r_j}{r_o}\right)^2\int_0^1\left(\frac{1}{\mu}\frac{u}{u_j} - \frac{\rho_j}{\rho_e \mu}\frac{\rho u}{\rho_j u_j}\right)\xi_1\,d\xi_1$$

$$= \left(\frac{r_j}{r_o}\right)^2\left\{\frac{1}{\mu}\int_0^1 \frac{u}{u_j}\xi_1\,d\xi_1 - \int_0^1\left(\frac{\rho_j}{\rho_e \mu}\frac{\rho u}{\rho_j u_j} - 1\right)\xi_1\,d\xi_1 - \frac{1}{2}\right\}$$

$$= \left(\frac{r_j}{r_o}\right)^2\left\{\frac{1}{\mu}\int_0^1\left[\mu + P_1\left(1-\xi_1^{3/2}\right)^2\right]\xi_1\,d\xi_1 - \frac{\rho_j}{\rho_e \mu}\frac{T_j R_j}{T_e \tilde{R}}\left(P_1F_1 - \mu P_2 F_3\right) - \frac{1}{2}\right\}$$

$$= \left(\frac{r_j}{r_o}\right)^2\left\{\frac{P_1}{\mu}\frac{9}{70} - \frac{1}{\mu}\left(P_1F_1 - \mu P_2 F_3\right)\right\} \qquad (B.8)$$

Hence, Eq. (B.3) becomes

$$\frac{1}{\mu}\left(\frac{r_j}{r_o}\right)^2\left[\frac{9}{70}P_1 - \left(P_1F_1 - \mu P_2 F_3\right)\right] = \frac{1}{2}\left(\frac{\tilde{u}_j}{u_e} - \frac{\tilde{\rho}_j \tilde{u}_j}{\rho_e u_e}\right)\left(\frac{\tilde{r}_j}{r_o}\right)^2 \qquad (B.9)$$

To solve Eqs. (B.5), (B.7) and (B.9) for the equivalent jet properties, let

$$f_1 = \frac{1}{\mu^2}\left(\frac{r_j}{r_o}\right)^2\left(P_1\mu F_1 + P_1^2 F_2\right) \qquad (B.10)$$

$$f_2 = \frac{1}{\mu}\left(\frac{r_j}{r_o}\right)^2\left(P_1F_1 - \mu P_2 F_3\right) \qquad (B.11)$$

$$f_3 = \frac{1}{\mu}\left(\frac{r_j}{r_o}\right)^2\left[\frac{9}{70}P_1 - \left(P_1F_1 - \mu P_2 F_3\right)\right] \qquad (B.12)$$

$$x_1 = \frac{\tilde{\rho}_j \tilde{u}_j}{\rho_e u_e} \qquad (B.13)$$

$$x_2 = \frac{\tilde{u}_j}{u_e} \qquad (B.14)$$

$$x_3 = \left(\frac{\tilde{r}_j}{r_o}\right)^2 \qquad (B.15)$$

Then,

$$2f_1 = x_1\left(x_2 - 1\right)x_3 \qquad (B.16)$$

$$2f_2 = (x_1 - 1)\, x_3 \tag{B.17}$$

$$2f_3 = (x_2 - x_1)\, x_3 \tag{B.18}$$

Solving Eqs. (B.16) - (B.18), it can be shown that

$$x_1 = \frac{f_1}{f_2 + f_3} \tag{B.19}$$

$$x_2 = \frac{f_3}{f_2}\left(\frac{f_1}{f_2 + f_3} - 1\right) + \frac{f_1}{f_2 + f_3} \tag{B.20}$$

$$x_3 = \frac{2f_2\,(f_2 + f_3)}{f_1 - f_2 - f_3} \tag{B.21}$$

For non-heated jets, $T_j = T_e$. In this case, Eq. (B.3) is not needed. The above solutions, Eqs. (B.19) - (B.21), are still applicable if f_3 is equated to zero.

Appendix C

Applications of Shanks' Transformation to Evaluation of Series

Consider the evaluation of the integral:

$$F_1 = \int_0^1 \frac{\xi_1 (1-\xi_1^{3/2})^2}{1 + P_2 (1-\xi_1^{3/2})} \, d\xi_1 \qquad (C.1)$$

Assuming small P_2, the following series can be obtained:

$$F_1 = \int_0^1 \xi_1 (1-\xi_1^{3/2})^2 [1 + P_2 (1-\xi_1^{3/2})]^{-1} d\xi_1$$

$$\cong \int_0^1 \xi_1 (1-\xi_1^{3/2})^2 [1 - P_2 (1-\xi_1^{3/2}) + P_2^2 (1-\xi_1^{3/2})^2 - P_2^3 (1-\xi_1^{3/2})^3 + P_2^4 (1-\xi_1^{3/2})^4] \, d\xi_1$$

$$= 0.1285714 - 0.089011 P_2 + 0.066758 P_2^2 - 0.052704 P_2^3 + 0.043121 P_2^4 \qquad (C.2)$$

By Shanks' transformation, F_1 can be rewritten as

$$F_1 \cong \frac{S_{n+1} S_{n-1} - S_n^2}{S_{n+1} S_{n-1} - 2 S_n} \qquad (C.3)$$

where S_n is the sum of the first n terms in Eq. (C.2). Since (n+1) terms are needed, n will be taken as 4 in Eq. (C.2). Therefore,

$$S_{n+1} = 0.1285714 - 0.089011 P_2 + 0.066758 P_2^2 - 0.052704 P_2^3 + 0.043121 P_2^4$$

After simplification, Eq. (C.3) gives

$$F_1 \cong \frac{0.12857 + 0.01617 P_2 - 0.00607 P_2^2 + 0.00192 P_2^3}{1 + 0.81817 P_2} \qquad (C.4)$$

Eq. (C.1) can be integrated exactly to give

$$F_1 = -\frac{2}{P_2} \left\{ \frac{9}{14} - \frac{7}{4} P_5 + P_5^2 + \frac{P_5}{P_2} \left[\frac{1}{6 P_5^{2/3}} \ln \frac{(1-P_5^{1/3})^2}{1 + P_5^{1/3} + P_5^{2/3}} + \frac{1}{\sqrt{3} P_5^{2/3}} \tan^{-1} \frac{P_5^{1/3} \sqrt{3}}{2 + P_5^{1/3}} - \frac{\pi}{3\sqrt{3} P_5^{2/3}} \right] \right\}, \quad P_5 = 1 + \frac{1}{P_2} \qquad (C.5)$$

Using Eq. (C.5) as the standard for comparison, Eq. (C.2) gives error of 22% while only 0.2% for Eq. (C.4) with $P_2 = 1.0$.